Naval Research Laboratory
Washington, DC 20375-5320

NRL/MR/6380--97-7997

Composite Piezoelectric Assemblies for Torsional Actuators

CHULHO KIM
TODD JESSEN
VIRGINIA DEGIORGI
BARRY BENDER
CARL CM WU
DAN FLIPPEN
DAVID LEWIS

Mechanics of Materials Branch
Materials Science and Technology Division

QIMING ZHANG
VOLKMAR MUELLER

Materials Research Laboratory
The Pennsylvania State University

MANFRED KAHN

Potomac Research, Inc.

RICHARD SILBERGLITT
L.K. LEN

FM Technologies, Inc.

September 30, 1997

REPORT DOCUMENTATION PAGE

Form Approved
OMB No. 0704-0188

1. AGENCY USE ONLY (*Leave Blank*)	2. REPORT DATE	3. REPORT TYPE AND DATES COVERED
	September 30, 1997	Progress Report, June 1996-July 1997

4. TITLE AND SUBTITLE

Composite Piezoelectric Assemblies for Torsional Actuator

5. FUNDING NUMBERS

DARPA Order #D752

6. AUTHOR(S)

Chulho Kim, Todd Jensen, Virginia DeGiorgi, Barry Bender, Carl Cm Wu, Dan Flippen, David Lewis, Qiming Zhang,* Volkmar Mueller,* Manfred Kahn,† Richard Silberglitt,† and L.K. Len‡

7. PERFORMING ORGANIZATION NAME(S) AND ADDRESS(ES)

Naval Research Laboratory
Washington, DC 20375-5320

Penn State University
University Park, PA 16802

8. PERFORMING ORGANIZATION REPORT NUMBER

NRL/MR/6380--97-7997

9. SPONSORING/MONITORING AGENCY NAME(S) AND ADDRESS(ES)

Defense Advanced Research Project Agency
Defense Science Organization
Arlington, VA 22203-1714

10. SPONSORING/MONITORING AGENCY REPORT NUMBER

11. SUPPLEMENTARY NOTES

*The Pennsylvania State University
†Potomac Research, Inc.
‡FM Technologies, Inc.

12a. DISTRIBUTION/AVAILABILITY STATEMENT

Approved for public release; distribution unlimited.

12b. DISTRIBUTION CODE

13. ABSTRACT (*Maximum 200 words*)

A new piezoelectric actuator was developed for the direct production of large angular displacement and torque, with a monolithic, solid state device. The intended application of this device is to control vibration and noise in aircraft, helicopter, spacecraft and in manipulators and positioners where direct rotary motion is required. Actuator design and assembly methods, materials preparation, poling procedures, and test results for joint strengths, and actuator output capabilities are discussed.

14. SUBJECT TERMS

Torsional actuator
Piezoelectric ceramics
Continuous poling
Shear strength
Conductive joint
Shear electromechanical properties

15. NUMBER OF PAGES

61

16. PRICE CODE

17. SECURITY CLASSIFICATION OF REPORT	18. SECURITY CLASSIFICATION OF THIS PAGE	19. SECURITY CLASSIFICATION OF ABSTRACT	20. LIMITATION OF ABSTRACT
UNCLASSIFIED	UNCLASSIFIED	UNCLASSIFIED	UL

CONTENTS

CONTENTS

(continued)

COMPOSITE PIEZOELECTRIC ASSEMBLIES FOR TORSIONAL ACTUATORS

1. OVERVIEW

The efforts here are intended to provide a basis for the utilization of novel electromechanical piezoelectric actuators and actuator configurations in smart materials and structures. The program addresses actuators and actuator configurations capable of amplifying integral strain and producing both large and small torsional motion. The efforts address the technologies for the preparation of such actuators and actuator materials, and draw on the extensive experience and expertise at NRL in such materials and devices. The modeling of actuator performance embedded in composite structures will be accomplished at NRL with assistance from other researchers at Penn State. NRL will also seek to establish teams with industry members suitable for accomplishing the required developmental efforts and for providing an eventual commercialization path for successful actuator configurations.

1.1 Overall Program Objectives:

The objectives of this program are: 1) to demonstrate that specially designed piezoelectric composite tubes can produce enough angular displacement and torque to control vibration and noise in aircraft, spacecraft, and other military and commercial structures; 2) to validate the concept of using multitube piezocomposite actuators in applications requiring large torque and angular displacement that can not be performed by a simple single tube design; and 3), in support of (1) and (2), to develop suitable poling techniques, conducting adhesives, and fatigue resistant joints for the torsional actuator assembly.

1.2 Tasks:

To accomplish these objectives, the following tasks are being implemented:

Task 1. Design, materials selection, segment preparation, and continuous

Manuscript approved August 27, 1997

poling

Task 2. Electroding and joining of a tubular actuator element

Task 3. Microscopic characterization and NDT analyses

Task 4. Element performance characterization

Task 5. Modeling for performance prediction

Task 6. Prototype actuator design, fabrication and testing

2. PROGRESS IN INDIVIDUAL TASKS

2.1 Design, Materials Selection, Segment Preparation, and Continuous Poling

2.1.1 Design of Tubular Actuator Element:

As a proof-of-concept, one of the many elements that would eventually form the actuator assembly has been designed as shown in Fig. 1.

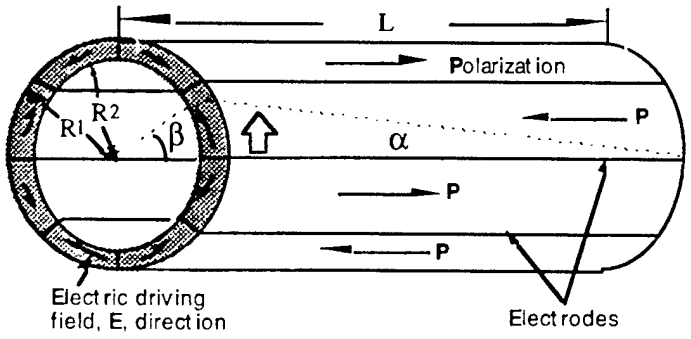

Fig. 1 Schematic of a torsion actuator element

Each element has been segmented and poled in such a way that the polarity alternates between adjacent segments. The segments are then joined with a conductive adhesive. As a result, application of a voltage to the assembled element should result in a torque, given by

$$F R = \frac{d_{15}\, n\, V\, (R_1 - R_2)}{s^E_{44}}\, R$$

Here the torque is a function of the voltage (V), the PZT type (d_{15}, s_{44}^E), the number of segments (n), and the tube wall thickness (R_1-R_2). For example, an 8-segment piezoelectric tube in an electric field of 4 kV/cm with d_{15} = 1,800 pm/V, s_{44}^E = 46 x 10^{-12} m^2/N, R_1 = 1.27 cm, R_2 = 0.95 cm, and an average radius of R = 1.11 cm will produce a torque of about 4,449 N-cm or 393 in-lb. This torque output is in between the torque required in the trailing edge flap (43±32 in-lb) and in the blade twist (±480 in-lb) in the rotor blade actuation of an eight-seated commercial helicopter.

An electric field on this basic torsion actuator element is also able to amplify small shear strains in each segment to large rotation angles in the element as a whole. One end of the element rotates by an angle β relative to the other end as described by the equation:

$$\beta = L\,\alpha / R$$

where $\alpha = d_{15}E$. If L > R, then $\beta > \alpha$ and an angular amplification is achieved. (See Fig. 1 for a graphic representation of the variables.) For example, with L/R = 50, E = 4 kV/cm and d_{15} = 1,750 pm/V, the actuator can produce a two-degree angle of twist which is in the range of the requirements in an eight-seated commercial helicopter (a twist angle in the trailing edge flap of ± 4° and a blade twist of ± 2° in the rotor blade).

2.1.2 Materials Selection

To determine the best ceramic for the Torsion Actuator Program, the shear response to an applied electric field and the load capability of the candidate PZT ceramic materials should be compared.

2.1.2.1 Evaluation of the Shear Electromechanical Properties Under Applied Electric Field

The best material should have the highest shear response under the limiting electric field (the field limit before depoling occurs) and a high sensitivity to applied electric fields. Under an external mechanical load, the material should have a low elastic shear compliance and a high depoling shear stress. The MRL of Penn State systematically examined the commercial PZT materials under a stress free condition to evaluate and characterize the non-linear shear response, the limiting electric field (E_{dp}), and the maximum shear strain (S_5^{max}). It can be shown that the maximum torsional angle (β) and the blocking torque (FR) can be expressed as

$$\beta = S_5^{max} L/R \quad \text{and} \quad FR = 2\pi S_5^{max} t R^2/s_{44}^E$$

where $S_5^{max} = d_{15} E_{dp}$ and $t = R_1-R_2$. In Table I, S_5^{max} and E_{dp} are listed for the materials tested.

NRL was provided two samples of EDO PZT-5A which were poled using a newly developed continuous poling set-up at NRL. From the results on these EDO PZT-5A samples tested at MRL, it is believed that as far as the shear piezoelectric response is concerned, the EDO PZT-5A is at least equivalent to Morgan PZT-5H. As can be seen in the table, EDO PZT-5A, PZT-5H and N-21 yield the highest S_5^{max}. EDO PZT-5A has the highest Curie temperature, thus, it was decided to work with the EDO PZT-5A tubes to produce a prototype device for the demonstration.

Also in the table are the results from two different test conditions: the continuous wave (CW) and the tone burst. It is seen that E_{dp} is higher for the tone burst case compared with the CW driving case. The results in Table I clearly show that the material with the best performance is neither the softest nor the hardest PZT.

Table I: Limiting field E_{dp} and field strain S_5^{max} of commercial PZTs

Material	E_{dp} (kV/cm)	S_5^{max} (10^{-3}) CW	E_{dp} (kV/cm)	S_5^{max} (10^{-3}) tone burst
PZT-8	>11	>0.4	19.8	0.75
PZT-4D	>9	>0.72	14.4	1.4
PZT-5A*	4.8	1.2		
PZT-5H	>4.9	1.1	8.9	2.5
N-21	6.2	1.2	>9.3	>2.75
3203HD	3.8	0.86	–	–
N-10	3.1	0.78	–	–

* EDO tubular PZT-5A

The test results also show that all the materials exhibit a large non-linear behavior and the effective d_{15} coefficient at high fields is much higher than that at low fields (see Fig. 2A and 2B). The d_{15} coefficient of EDO PZT-5A at 4 KV/cm is 2300 pC/N as compared to 700 pC/N at low fields (<200 V/cm). The experimental results show that the non-linear behavior of the d_{15} coefficient can be expressed as

$$d_{15} = Q_{eff} (\chi_{lin} + \chi_{nlin} E_{am}^{1.5})$$

where χ_{lin} and χ_{nlin} are the linear and non-linear dielectric responses. The fractional exponent of 1.5 indicates that the domain wall motion in these ceramics can be modeled as an interface pinned by random defect fields.

Additionally, there is a direct link between the linear part χ_{lin} and the non-linear part χ_{nlin} of the dielectric constants as shown in Fig. 3A. For a soft PZT, in which χ_{lin} is large, the non-linear part is also correspondingly large. There is also a linear relationship between the strain response as represented by Q_{eff} and the linear dielectric response as shown in Fig. 3B.

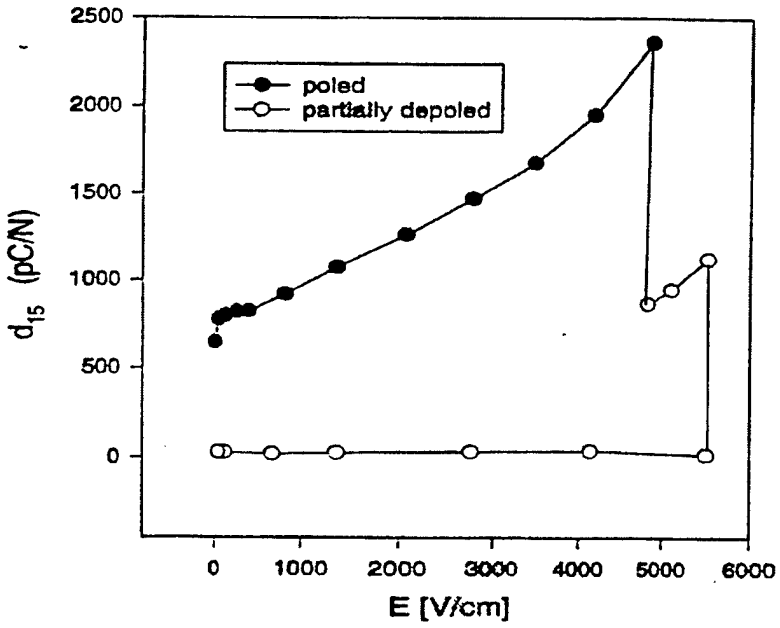

Fig. 2A d_{15} shear coefficients of PZT-5H with applied electric field

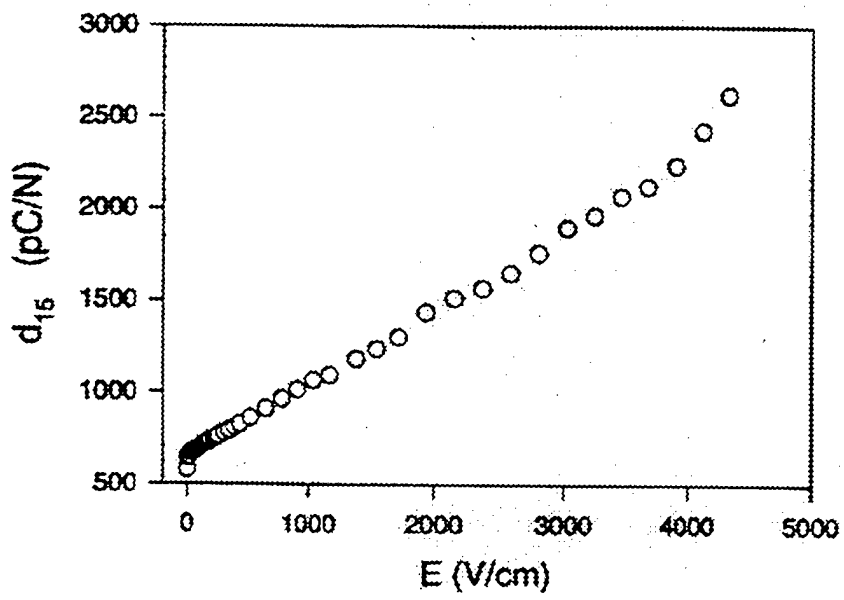

Fig. 2B d_{15} shear coefficients of EDO PZT-5A with applied electric field

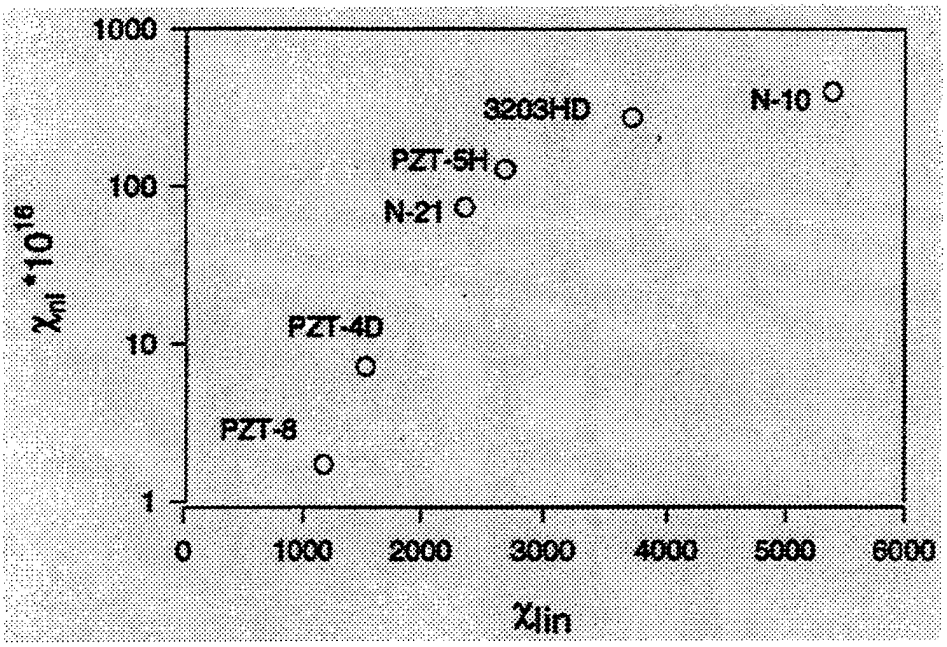

Fig. 3A Linear coefficients vs. nonlinearities of tested PZT materials

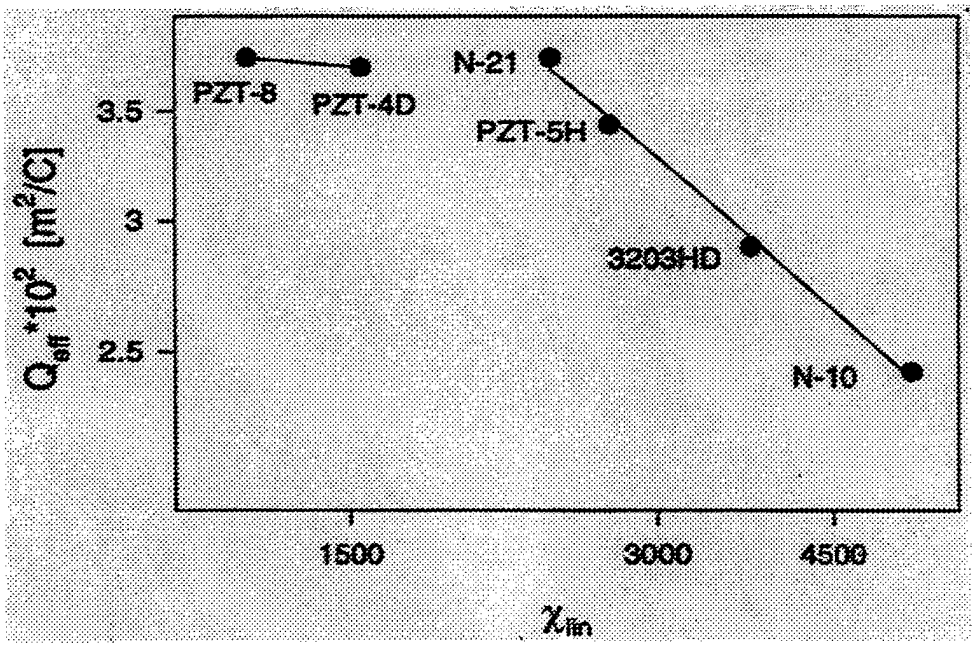

Fig. 3B Strain response, Q_{eff} , vs. linear dielectric response, χ_{lin} Q_{eff}

Apparently, the hard PZTs behave differently from the soft PZTs.

To compare piezoelectric shear performance, the d_{15} of several commercially available PZT piezoceramics was plotted against their respective d_{33} as shown in Fig. 4. Clearly, EDO PZT-5A, Token N-21, and Motorola 3203HD have a higher ratio of d_{15}/d_{33} compared with the other PZT materials. Hence, EDO PZT-5A seems to be a good choice for the current torsional actuator. These results can be valuable in guiding the future modeling of the device under high driving fields.

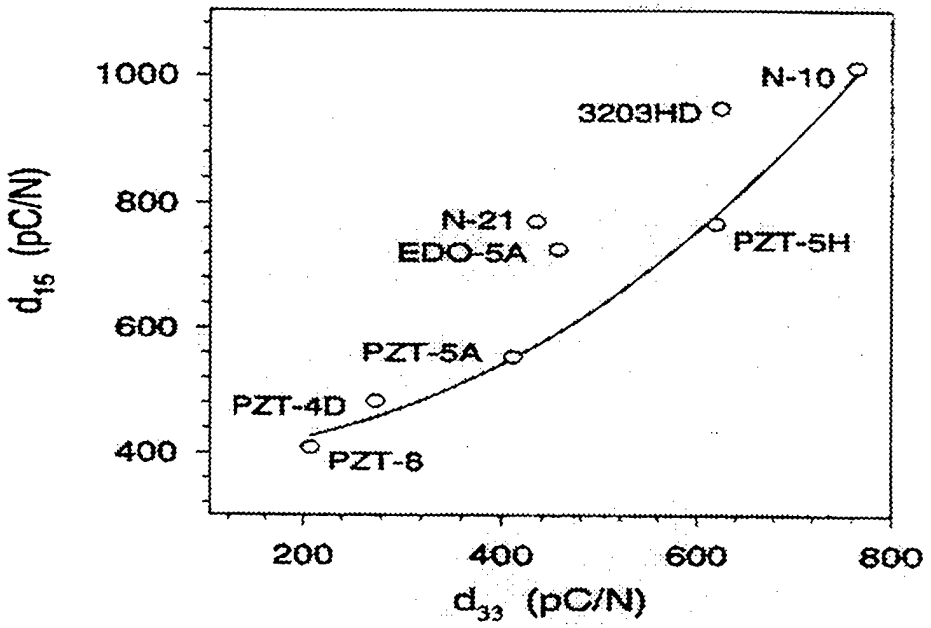

Fig. 4 Comparison of d_{15} and d_{33} of commercial PZT materials

From the results, it also appears that the current commercially available PZT piezoceramics are not optimized for their shear piezoelectric response. Most of the current PZT piezoceramics are optimized for their tensile piezoelectric properties and the domain mechanisms for the tensile and shear piezoelectric responses are different. It would be worthwhile to carry out an investigation on optimization of the piezoelectric shear response in PZT ceramics. From the domain pattern most suitable for the

piezoelectric shear response, it seems that a grain oriented piezoceramic would yield the best shear response.

2.1.2.2 Evaluation of the Shear Electromechanical Properties under Shear Loading Condition

One of the concerns in using piezoceramic materials for a broad range of actuator applications is the performance of the materials under load conditions. Although it is a very important design concern, the data are scarce for most of the piezoceramic materials. The reason for that is the difficulty of the experiment because of the small sample size and displacement levels (about 100 micro-strain in most cases). Hence, a reliable technique to perform shear load testing on piezoceramic material was developed where the change of the load is provided by a Universal Test Machine. In this apparatus, used to convert a tensile load into a shear load, the crucial part is to keep the stress in the test sample as pure shear. In order to achieve that, several steps in the technique have been modified, ranging from the design of the sample holder to the preparation of test samples.

The piezoelectric shear constant, d_{15}, the dielectric constant, ε_{11}, and the shear elastic compliance, s_{44} , were measured as a function of shear load, T_4. Not much change in s_{44} with the shear load was observed which seems to parallel the observations in the tensile load situation where the variation in the tensile elastic compliance is much weaker than that of the piezoelectric constants (d_{33} and d_{13}) and the dielectric constant, ε_{33}. Presented in Fig. 5A and 5B are the results of the test for EDO PZT-5A . The highest stress applied in the test was about 10 Mpa. At higher stresses the samples either depoled or fractured. The relatively low fracture strength observed in these materials may not be the intrinsic shear strength since we cannot rule out the existence of small flaws whose influence is magnified in the flexural test.

However, for EDO PZT-5A, in the stress range tested, there is no marked change of d_{15} with respect to the load stress, T_4, as shown in Fig. 5A and 5B. From the data, it can be deduced that the EDO PZT-5A actuator can generate at least 8 MPa shear stress and hence, a torsional actuator with the dimensions shown in Fig.1 (R=0.5" and thickness=0.125") can generate a torque of 2400 N-cm, which is larger than what was expected from the previous calculation. The reason is that the material has a large piezoelectric non-linearity which increases the d_{15} significantly in a high driving field. Combining the data in this section and section 2.4.2, it can be concluded that the performance of the d_{15}-based torsional actuator is better than predicted.

2.1.3 Segment Preparation:

Piezoelectric ceramic segments for the assembly of single tube actuator elements can be prepared by casting, injection molding, or cutting. For the proof-of-concept demonstration, PZT-5A tubes were cut longitudinally into eight equal segments using the fixture in Fig. 6. The PZT tube cutting procedure was as follows:

O-rings were placed in the four grooves in the aluminum rod. Two PZT tubes were slid along the rod and the spacing, created by the O-rings between the rod and the tubes, was checked for uniformity. The gap between the rod and the tubes on either side of the O-rings was filled with wax to secure the tube in place. The PZT tubes were cut longitudinally with a diamond saw every 45° on the circumference to produce eight segments. As-mounted and cut, two PZT-5A tubes are shown in Fig.7A. Using a 12 mil thick diamond wheel, the estimated loss of material was about 15 mils in each cut as evidenced by the reduction of the average outer diameter of the tubes from 2.70 cm (1.06 in.) to 2.60 cm

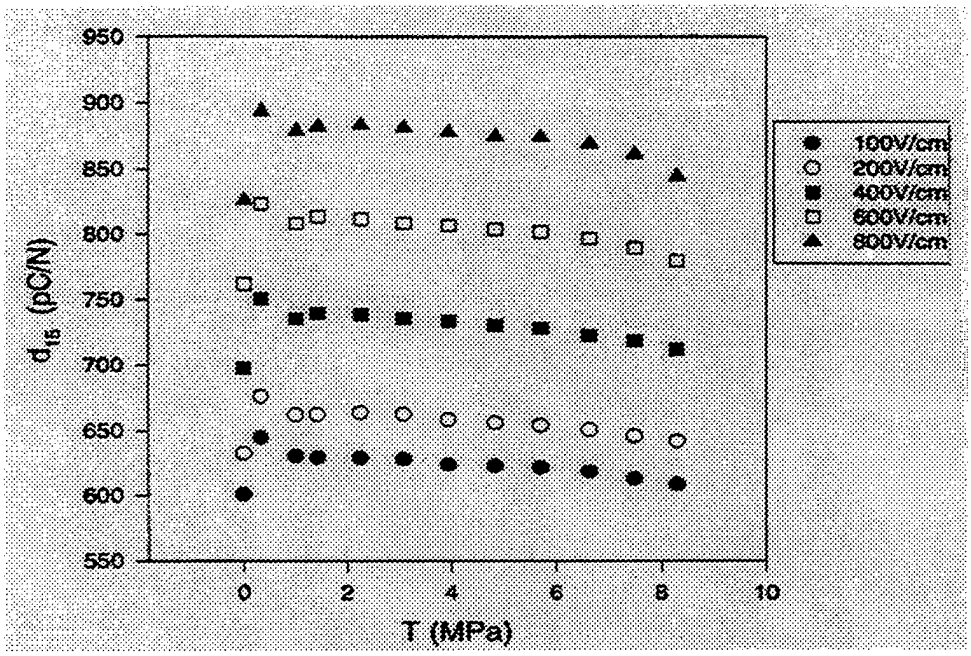

Fig. 5A Results of d_{15} under load T_4 for EDO PZT-5A

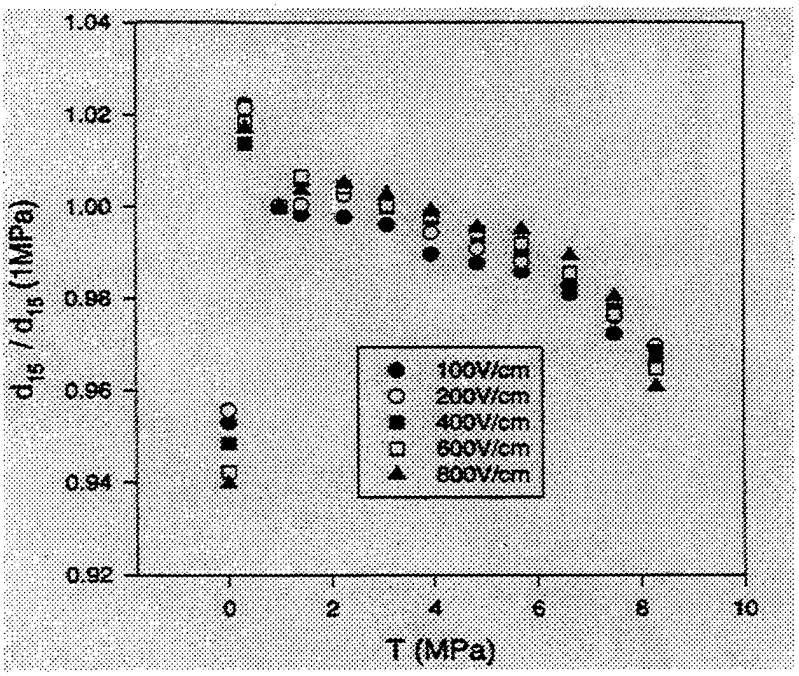

Fig. 5B Results of d_{15} under load T_4 for Edo PZT-5A(Normalized to d_{15} at 1 MPa).

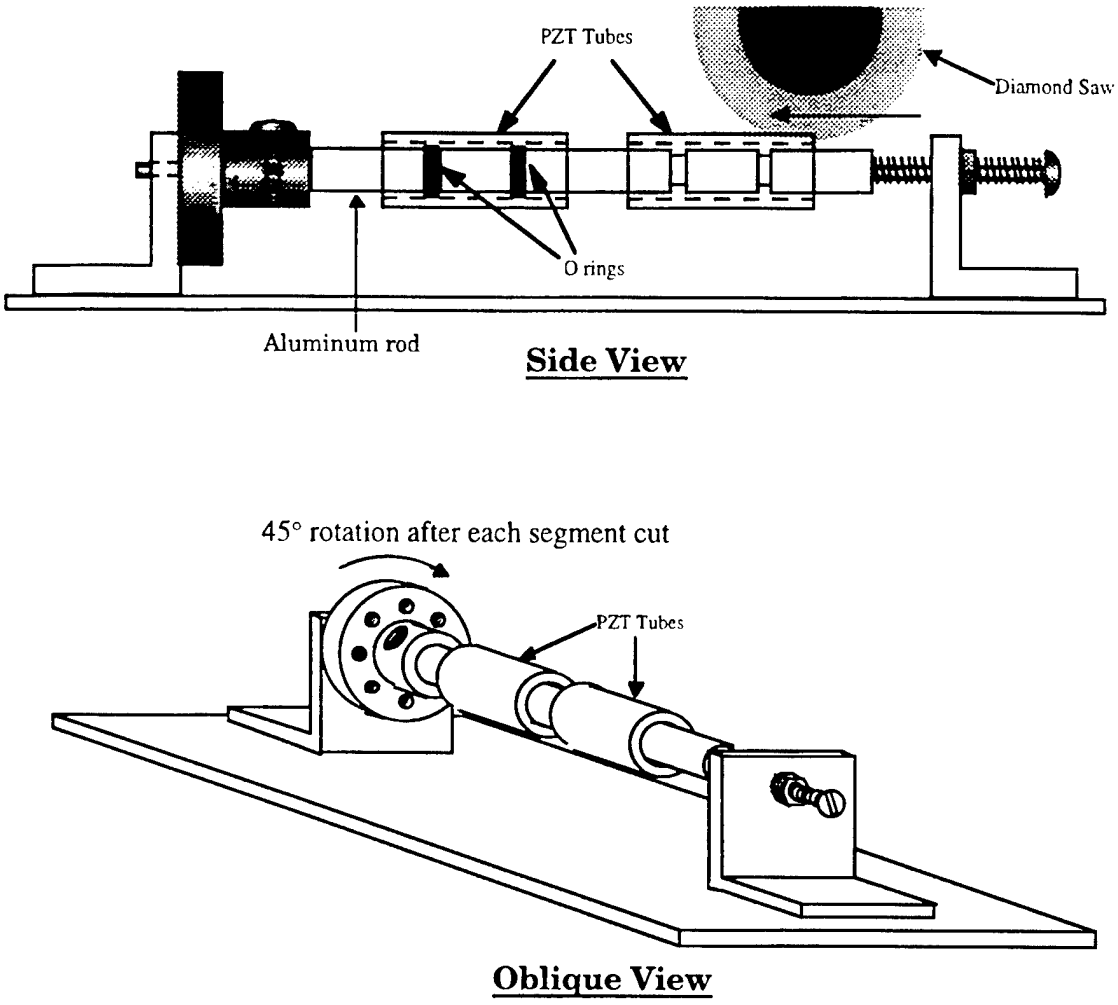

Fig.6 Schematic of the segment preparation fixture.

(1.02 in.). It should be noted that, in order to obtain the best cut surface finish, the depth and speed for each cutting pass had to be carefully determined. The segments cut from two tubes are shown in Fig. 7B (outside displayed on the left, inside on the right). To demonstrate the smoothness of the cut and the tight fit between the castellated tube ends, the segments were assembled and held in position with tape, as shown in Fig. 7C.

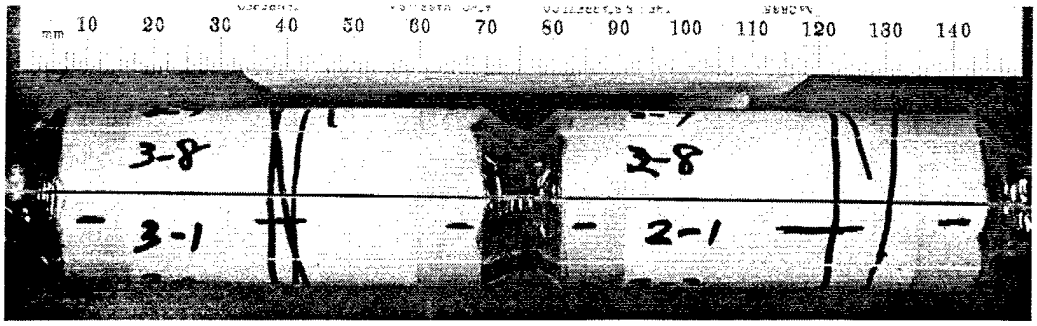

Fig. 7A As-mounted and cut two PZT-5A tubes

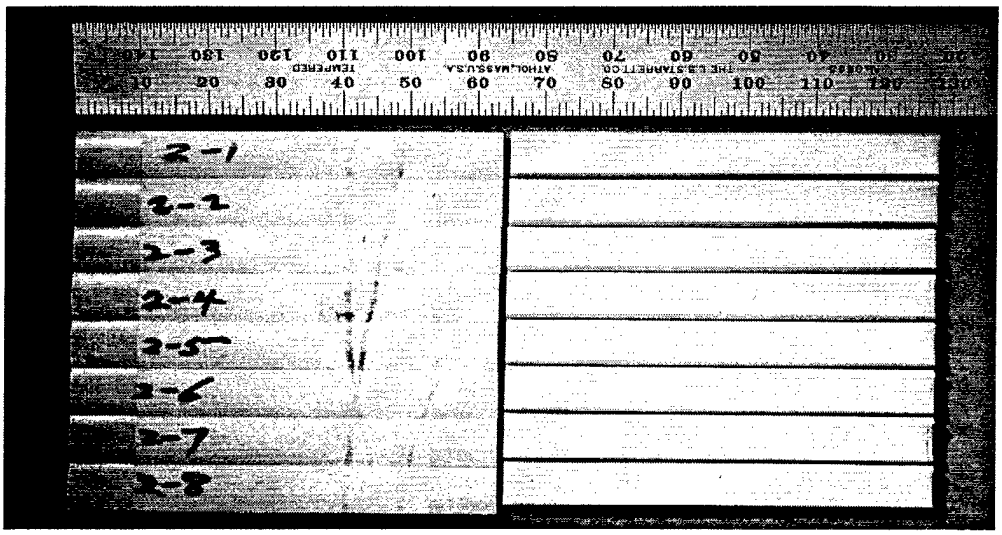

Fig. 7B Sixteen segments prepared using diamond saw cutting.

2.1.4 Continuous Poling:

The poling of slender segments requires a trade-off between the minimum electric field strength necessary to approach full uniform poling and the maximum field strength to avoid material failure. Guided by this concept, a continuous poling technique was developed and two slightly different fixtures were made. Either fixture can handle larger segments than the ones poled to date; however, only the details of the poling of slender segments are reported here. Two and one-half inch (6 cm) long

PZT-5A segments have been continuously poled to more than 95% of the maximum measured d_{33} as shown in Fig. 8 using the continuous poling device shown in Fig. 9.

This device can be used to pole one to four segments at a time by using a multi-sample poling electrode configuration as shown in the right sub-set of Fig. 9. The long segments are held by the metal specimen holder and the conductive rubber electrodes (co-linear slits separated by a distance of 1.2

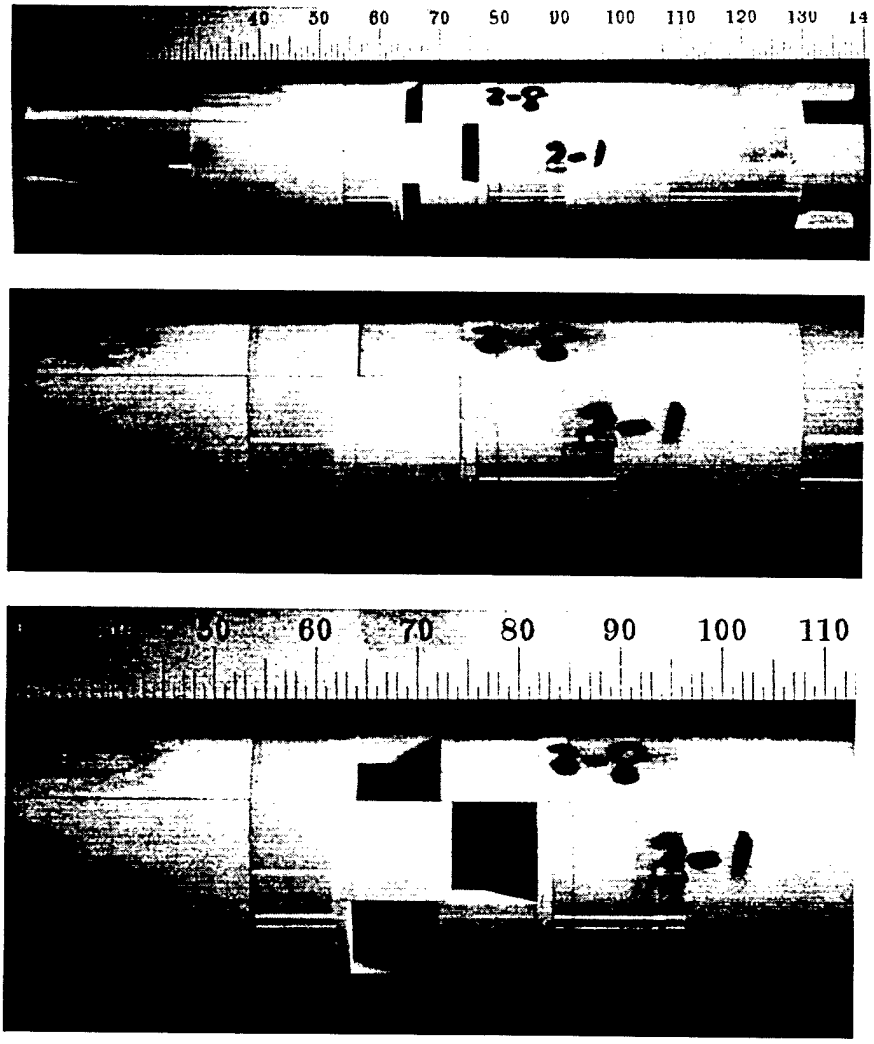

Fig. 7C Two assembled (with tape) tubes tightly fit into each other sliding in and out smoothly.

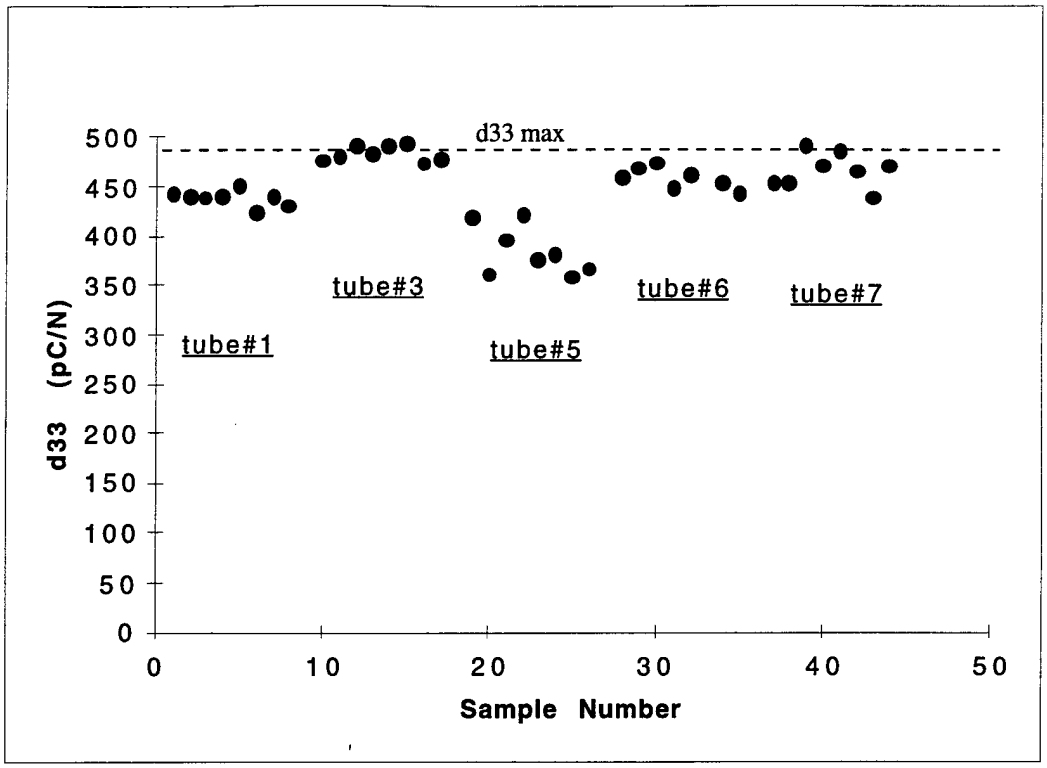

Fig. 8 Piezoelectric constant, d_{33}, data of the continuously poled EDO PZT-5A segments from five 6 cm-long tubes.

cm) are slid along the length of the sample at 0.2-1.0 cm per minute speeds (after a desired electric field is applied at one end). The entire system is immersed in a dielectric oil bath heated to 80-100 °C.

The dependence of polarization (d_{33}) on poling parameters was systematically determined experimentally using the conventional non-continuous poling technique. Polarization is not very sensitive to either temperature (in the range from 70 to 110 °C as shown in Fig. 10) or poling speed (in the range from 2 to 10 mm/min.). However, the polarization is dependent on the applied field as shown in Fig. 10 and 11 from which it may be seen that at a field strength of 14 kV/cm a polarization of more

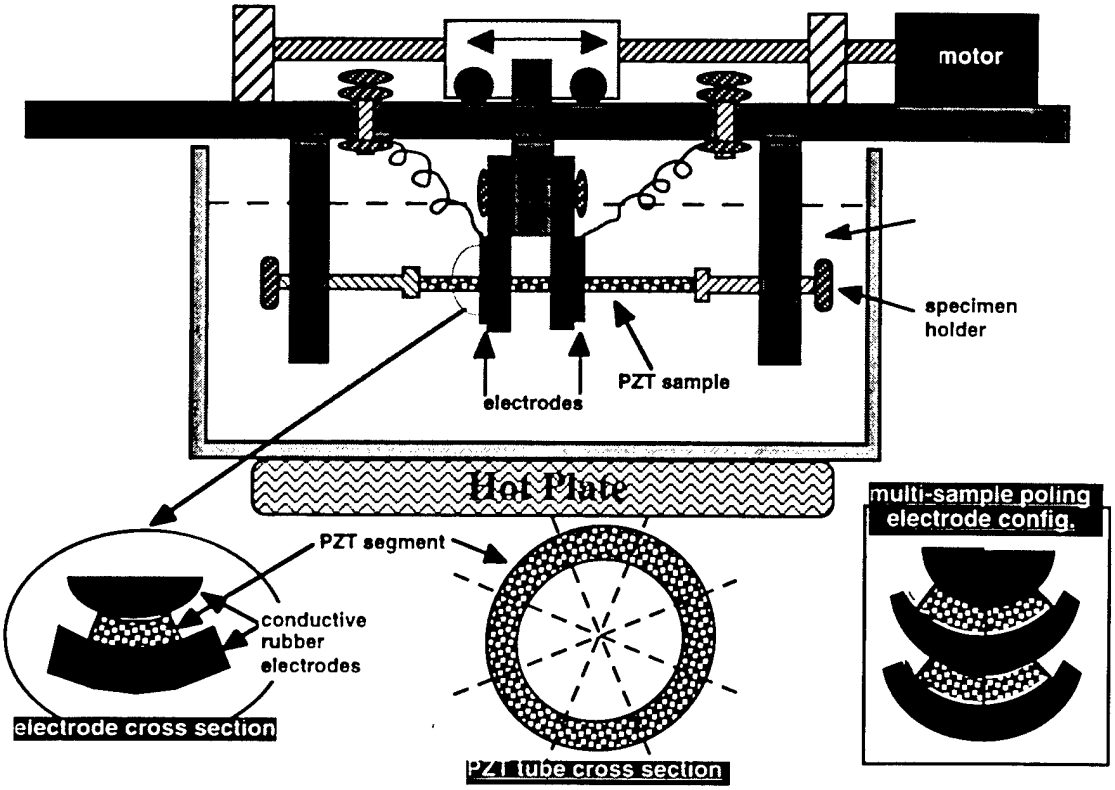

Fig. 9 Schematic of continuous poling fixture

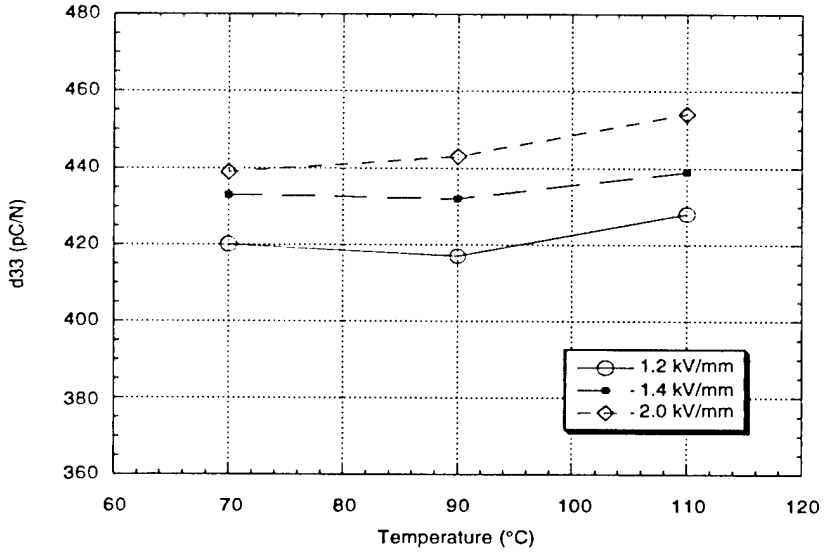

Fig. 10 Poling temperature dependence of piezoelectric strain constant, d_{33}, of EDO PZT-5A (data points are averaged values)

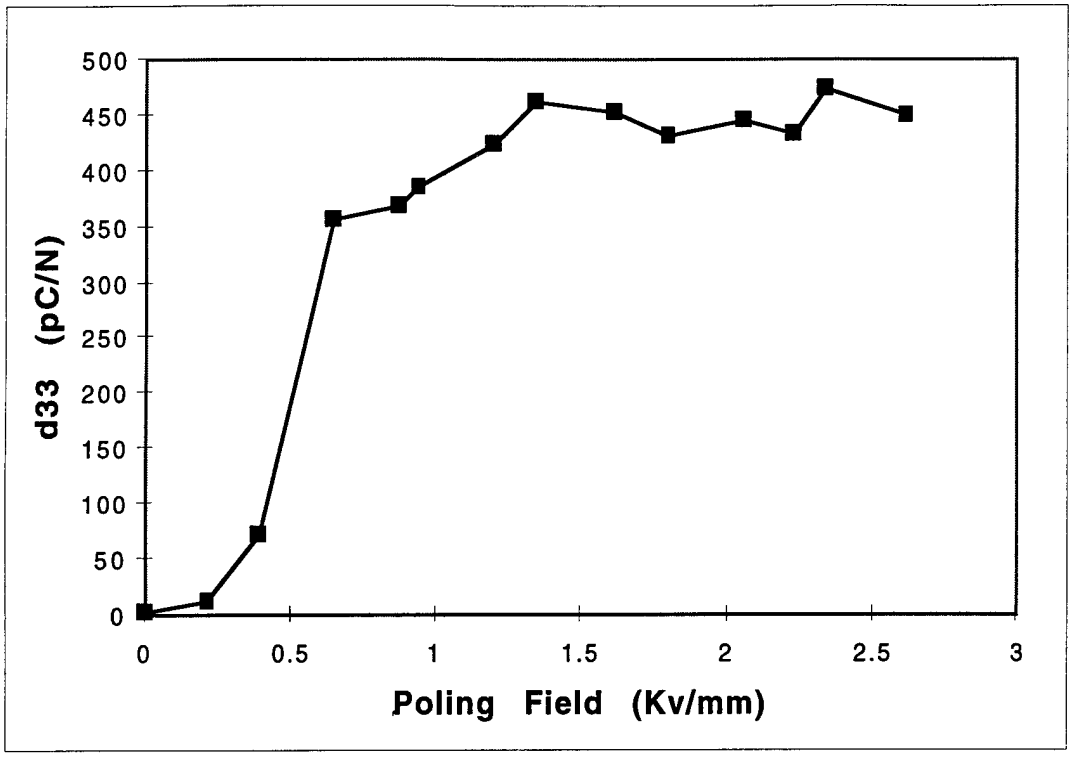

Fig. 11 Poling field strength dependence of piezoelectric strain constant, d_{33}, of Edo PZT-5A segments poled across its thickness (3.2 mm).

than 95% (440 pC/N) of the known measured maximum (470 pC/N) has been reached. The chosen separation distance between electrodes for the segment thickness used was guided by predictions from the electric dipole model* (Fig.12A) which has been qualitatively validated in Fig. 12B. The two surface electrodes, shown in the sub set of Fig. 12A, were treated as an electric dipole with positive and negative charges of equal magnitude to calculate the electric field E' inside the ceramic along the perpendicular bisector of the two electrodes as a function of depth r, thus

$$E' = E\, a^3 / (a^2 + r^2)^{3/2}$$

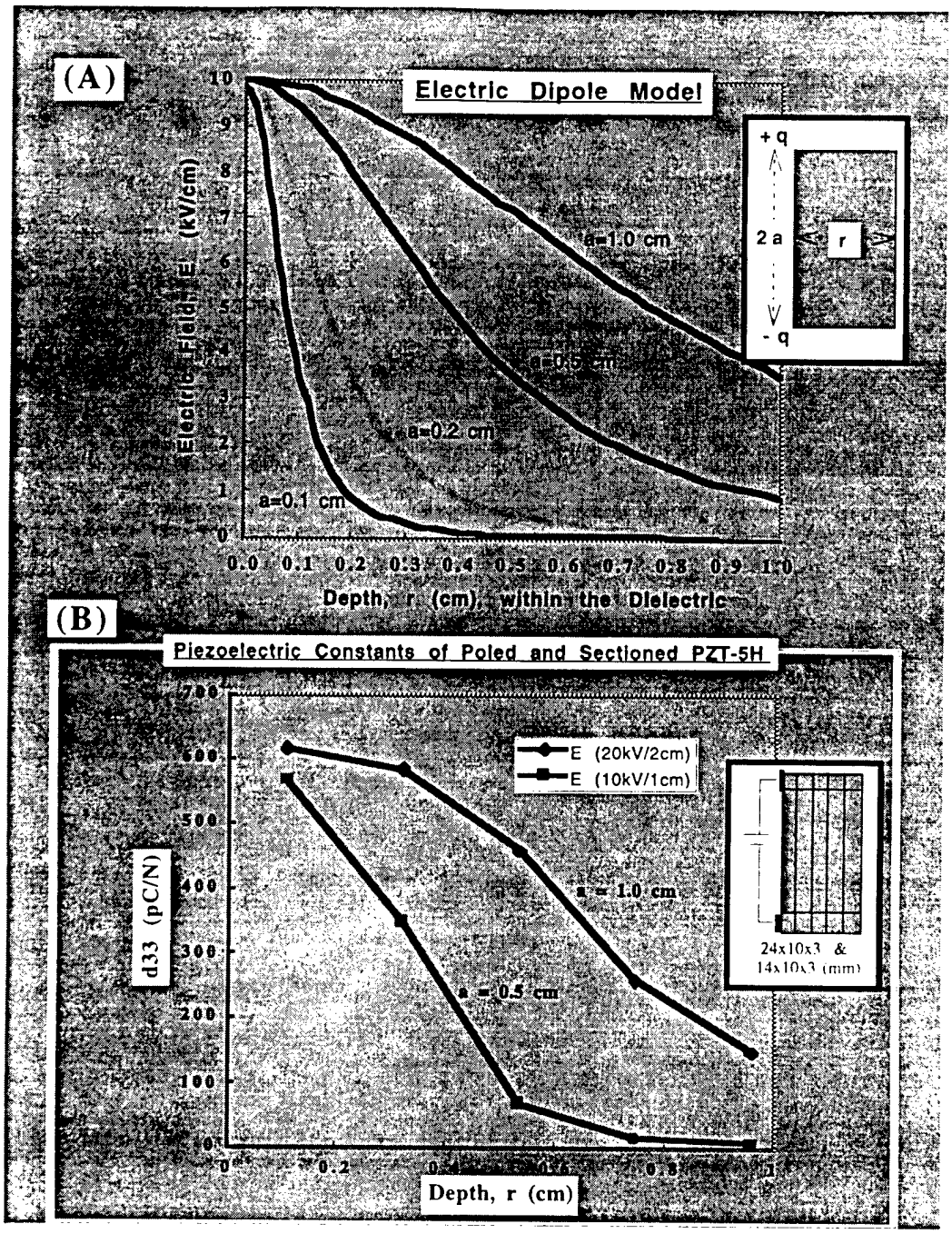

Fig. 12 (A) Electric dipole model: electric field strength inside the dielectric material as function of electrode separation and bisect depth distance. (B) Experimental data: measured d_{33} of the sectioned PZT-5H as function of depth distance, r, for electrode separations of 2a =1 and 2 cm.

where 2a is the electrode separation, r is the distance below the surface and E is the applied electric field at the surface (r=0). This figure illustrates that the electric field at a given depth inside the ceramic is higher for larger electrode separation when the applied electric field is the same (i.e. $E'_{(20kV/2cm)} > E'_{(10kV/1cm)}$). Experimental data in Fig. 10B shows the measured d_{33} of the sectioned PZT-5H as a function of depth distance, r, for samples poled with E=10 kV/cm and for electrode separations of 2a = 1 and 2 cm. The poled PZT-5H samples were sectioned into five pieces with two (2) mm thick pieces and shortened at each end by a length equal to an electrode width. Therefore the piezoelectric d_{33} coefficients measured in each piece represents a degree of poling due to an average electric field applied to each section.

2.2 Electroding and Joining of Segments into a Tubular Actuator Element

One of the critical issues in this project is to have good conductive joining of the poled segments to assemble them into the tubular actuator. In this task, surface preparation, joining materials and methods, and their effects on the tubes' mechanical properties are investigated.

2.2.1 Effect of Cutting Depth and Speed on Tube Shear Strength of Joined Segments

NRL conducted a preliminary investigation on how to accomplish the best electroding and joining of segments into a tubular actuator element for tests on the actuator's performance. There were three primary studies.

1) Machining studies were conducted on both PZT-4D (Morgan Matroc) and PZT-5A (EDO) materials to determine the effect of cutting depth/speed on surface finish. Four conditions were considered: (a) 0.001"/pass-manual feed, (b) 0.005"/pass-manual feed, (c) 0.005"/pass-

automatic feed, and (d) 0.030"/pass-automatic feed. SEM observations and profilometry confirm that condition (a) yields the 'roughest' surface and condition (d) the 'smoothest'.

2) A series of epoxy bonding materials were evaluated for their handling, wetting, and resultant joint thickness. Spurr™ epoxy was selected for the initial joining experiments because of its ability to form thin, strong bonds. An alternative joining scheme involving a multilayer deposition of various metals was considered. A source to provide candidates for the proof-of-concept demonstration of the latter option is being sought.

3) A series of shear test specimens were prepared to evaluate both the machined surface finish and the joining condition. For these studies, only PZT-5A material was used. Shear testing was used to evaluate the joint integrity because of the anticipated stresses during actuation. Two surface finishes were investigated: 0.001"/pass-manual feed and 0.030"/pass-automatic feed. Three joint conditions were evaluated: (a) epoxy only, (b) epoxy with air-dried Ag electrode, and (c) epoxy with sputter-deposited Au electrode.

Specimen handling and curing fixtures and methodology were developed to provide aligned sandwiched structures. Connectivity and conductivity measurements were made on a series of Au sputtering conditions to determine the best deposition time for continuous coatings. Three sandwich units were tested for each condition listed above and the results are shown in Fig. 13.

In summary, the results were: 1) 0.001"/pass-manual feed machining provided the strongest bond for all joint conditions; 2) Only epoxy provided the strongest bond for both surface conditions. Sputtered Au coatings with epoxy exhibited significantly more ceramic pullout than the air-dried Ag/epoxy joints. However, the Au and Ag joints within each machining finish had statistically-equivalent shear strengths; 3) All joint failures were

brittle. This is good in that the joint would not absorb actuation, however, brittleness may cause failure during actuation.

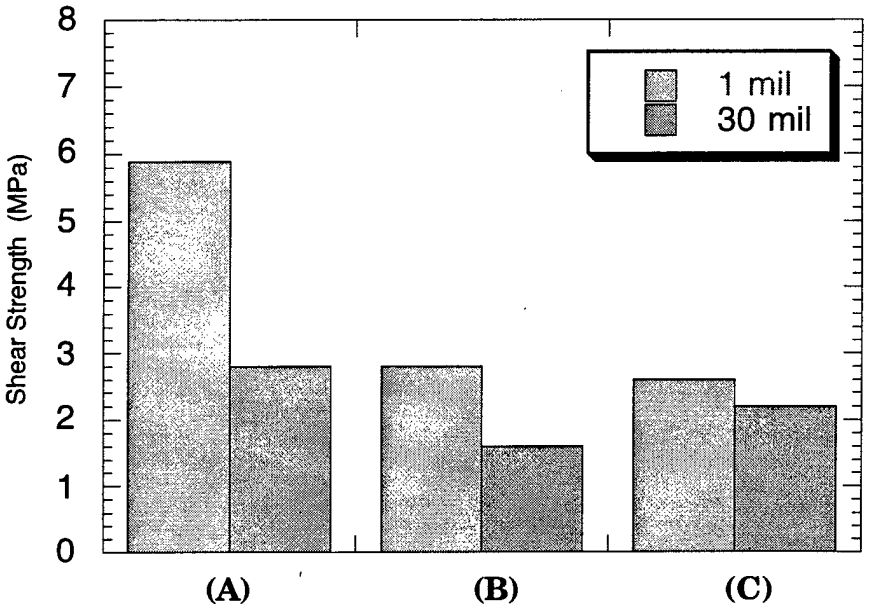

Fig. 13 Comparison of shear test of samples with different joining conditions: (A) Epoxy only, (B) Epoxy/Ag interface, and (C) Epoxy/Au interface.

2.2.2 Evaluation of the Conductive Epoxy and Modified Primer

There are variety of ways to join PZT ceramic segments and to provide the necessary electrical conductivity. The surfaces of the elements can be coated with a conductive material (e.g. by sputtering a gold film) and then joined with adhesive or conductive adhesive compounds. Currently, we are using conductive adhesives for their simplicity, availability and cost.

The two compounds that were chosen are:

- TRA- CON adhesives, catalog # TRA-DUCT 2902 and 2922. These are silver filled, electrical conductive epoxies.
- CYTEC system, BR 127. This was actually developed as a primer for surface coating. It consists of epoxy/phenolic resins with curing agents in

the solvent. Silver powder of 0.7-1.3 micron size is added before use to provide electrical conduction.

Using Tra-con Epoxy, the surfaces of the actuator elements were cleaned and joined. Curing can be either at room temperature or at an elevated temperature (65-110 °C) with light pressure. Using the Cytec primer, the BR 127 compound was applied and left to dry on both surfaces for about 10 minutes until tacky to the touch. The parts were then joined and light pressure was applied while curing at 125 °C for one hour.

It is important to evaluate the shear strength of the above joints to make sure that they will perform as required. The measurement was performed using a double shear test technique developed at NRL. A pair of joints were sheared in the tester by a loading blade in an Instron Testing Machine with a loading rate of 0.5 mm/min. The shear strength can be calculated as $S = 9.8\ P/2A$ MPa where P is the fracture load in kg and A is the sheared area in mm^2. Shear strength was also measured for plain EDO PZT-5A as a reference.

The resultant shear strengths of various joints are listed in Table II. The shear strengths for Tra-con epoxy on aluminum to aluminum at various curing temperature are shown in Table III.

It is noted that except for the joints that were made with only BR 127 primer without silver or made on surfaces with fused silver electrodes, all of the failures of the shear tests were through the PZT ceramic body. Through examination of the test results, the manufacturer's data, and the fact that fracturing occurred through the PZT, the shear strength of those joints is higher than the shear strength of the PZT.

A conclusion that can be drawn from these tests is that the two joining compounds, the joining techniques, and the shear strength of the joints are acceptable for the Torsional Actuator Program. However, joining needs improvements in the areas of thickness control and the procedure itself so that uniform joints can be produced.

Table II SHEAR STRENGTH OF PZT-5A JOINTS

- Shear strength of EDO PZT 5A — 15 ± 5 Mpa
- TRA-CON bond
  - Joint thickness: 25 μm
  - Shear strength — 13 ± 3 MPa
  - Fracture mode: through PZT
- Cytec bond
  - Joint thickness: 25-50 μm
  - Shear strength — 17.6 ± 6 MPa
  - Fracture mode: through PZT
- Cytec bond (primer only, no silver)
  - Shear strength — 16. ± 1 MPa
  - Fracture mode through joints
- Cytec bond on fired-on silver surfaces (primer only)
  - Shear strength — 6.7 ± 2 MPa
  - Fracture mode: through joints

Table III TRA-CON: ASTM D1002 SHEAR TEST

as reported by Tra-con

24 h @ 25 C	4.8 MPa (700 psi)
2 h @ 65 C	6.9 MPa (1000 psi)
1 h @ 110 C	11 MPa (1600 psi)

2.2.3 Evaluation of Pulsed Induction Joining of PZT Segments

Another approach using higher temperature brazing materials is being initiated by FMT. Incusil®-ABA™ is an active brazing alloy (Cu-Ag-Ti) with a liquidus temperature of 715°C, well above the Curie Temperature of the PZT. One of the benefits of the pulsed induction joining approach is its ability to produce a peaked temperature profile with the possibility of holding the bulk of the PZT specimen below the Curie point during joining. Some initial experiments using Au-coated PZT and Au-coated Mo or Nb were performed. The Mo or Nb pulsed induction heating layer was used with braze on either side. The specimen was heated rapidly (20 seconds) to a temperature above the liquidus of the brazing alloy and the materials were observed to be joined, but problems with wetting led to weak bonding. Analysis at NRL of the specimen that was debonded from the weak joint showed a variation of d_{33} with distance from joint. (d_{33} was zero for the first 2 mm, 50 pC/N between 2 and 5 mm, and 350 pC/N 5 mm from interface.) A low temperature brazing alloy, (80Au/20Sn, T_B = 280 °C), will eliminate the depoling problem and there are planned experiments with Cr and Ni sputter deposited PZT surfaces.

2.3 Microscopic Characterization and NDT Analysis

Microstructural characterization and electric impedance measurements were conducted on the assembled actuator tubes to ensure the joint integrity and to evaluate the joining procedure.

2.3.1 Microstructural Characterization of Bonded Joints

Two different types of bonds were investigated as follow:

A) Commercial Silver Epoxy-Bonded Joints

The joints were coated with a commercial silver epoxy (TRA-DUCT 2902) and were pressed together by hand. As a result of being hand-

pressed, there was a large variation in the thickness of the silver epoxy joint. This variation in thickness of the joint can be seen in the SEM micrograph of a polished cross-section of the joint (Fig. 14(A)). Typically, the thickness of the joint varied from 10 to 30 μm with a representative thickness of 25 μm. In Fig. 14(B), one can see that the thin silver plates partially aligned themselves perpendicular to the pressing direction. Fig. 14(C), which is a back-scattered electron image of the epoxy/PZT interface, shows that epoxy wets the PZT joint well. SEM also indicated that there were no observable differences in the joint microstructure between a sample that had been joined and poled and sample that had not been poled.

Fig. 15 are SEM fractographs of a joint that had fractured during the slicing operation. Fig. 15(A) shows that the sample fractures are through the silver epoxy itself and not at the silver epoxy/PZT interface. In Fig. 15(A) air pockets can be observed in the silver epoxy. Fig. 15(B) shows these air pockets in greater detail as well as showing the thin platelets of silver on the fracture surface.

B) Silver-Loaded BR 127 Primer-Bonded Joint

BR 127 epoxy loaded with silver powder (17% volume) was the bonding precursor used for joining these PZT sections. Two types of bonded-joints were fabricated. 'B' joints were made by applying the precursor to both surfaces of the PZT sections to be bonded, while 'N' joints were made by applying the precursor to only one of the surfaces of the PZT section to be joined. Macrographs of an assembled PZT-5A torsional actuator tube using Ag-loaded BR 127 epoxy are shown in Fig. 16. Consolidation of this joint was done by vacuum bagging the sections. Bonded sections broken by hand for both B and N joints had similar fracture surfaces. The fracture surface is very irregular (Fig. 17(A)) ; the joint tears apart in no particular

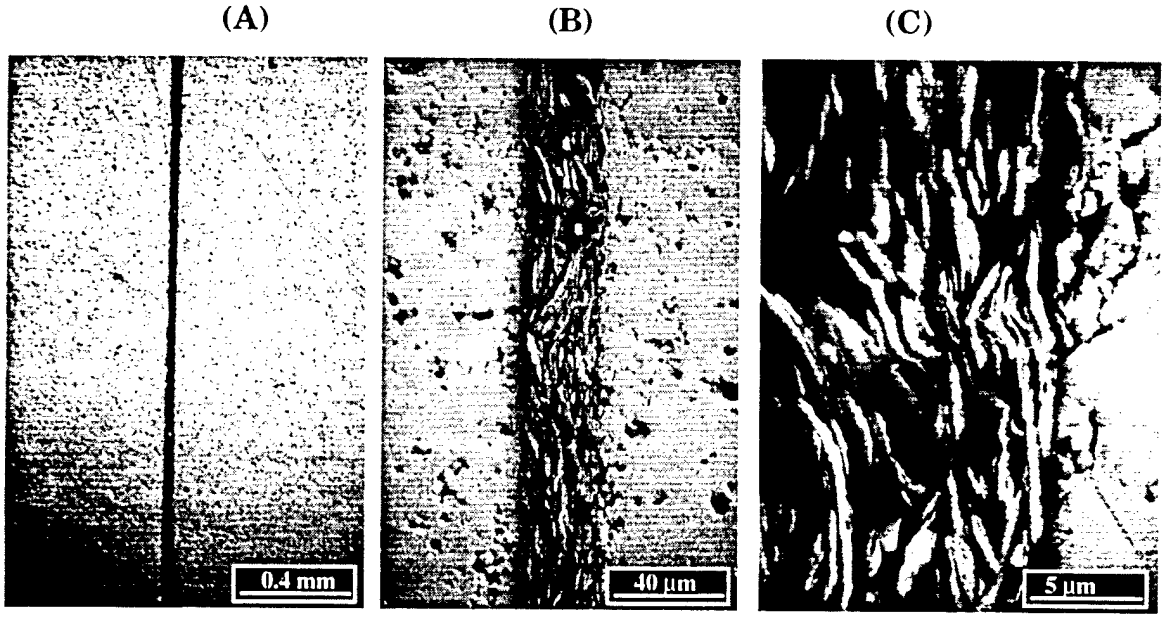

Fig.14 SEM micrographs of a polished cross section of a joint bonded with Tra-con 2902

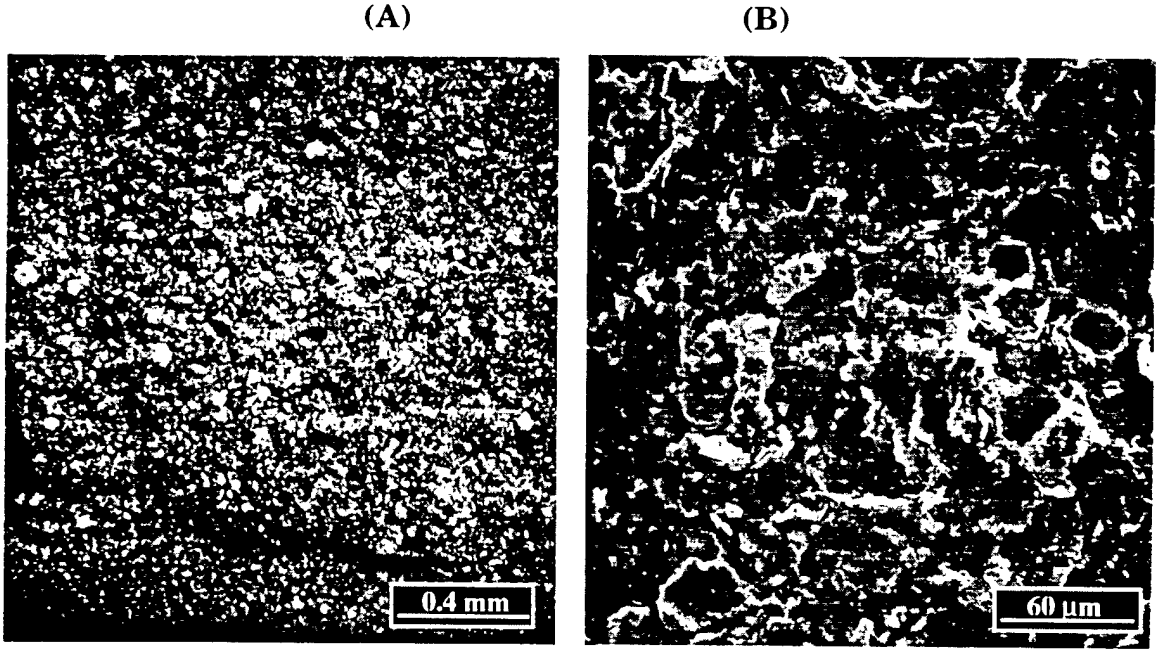

Fig.15 SEM micrographs of the fractured surface of a joint bonded with Tra-con 2902

manner as there are areas where the joint fails at the epoxy/PZT interface and the epoxy itself. Fig. 17(B) shows that the fracture surface is very rough and irregular especially compared to the fracture surface of the commercial silver epoxied-joint (Fig. 15(B)). Also in Fig. 17(B) the added silver powder can be seen as small bright clumps. Also holes are seen in the fracture surface; they may be holes left behind from pullout of the

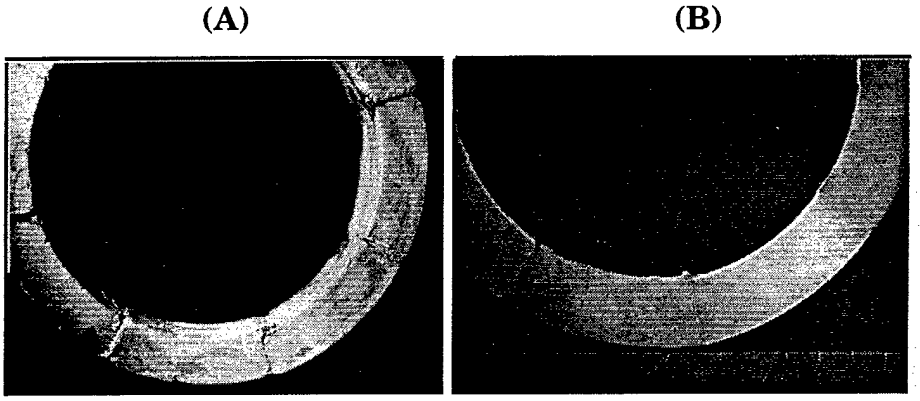

Fig.16 Assembled PZT-5A torsional actuator tube showing; (A) end view, and (B) cross section view

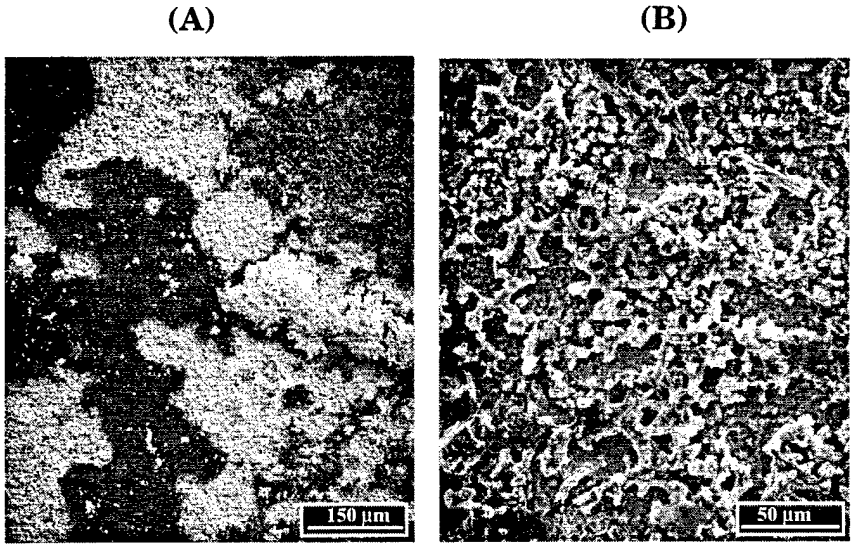

Fig.17 SEM micrographs of the fractured surface of a joint bonded with Ag powder loaded BR127 epoxy

clumps of silver powder during fracture or they may be pores that developed during the curing of the epoxy.

Consolidation of the joints by vacuum bagging leads to joints whose thicknesses are a lot more uniform along the length of the joint as shown in Fig. 18(A). Fig. 18(B) shows that the N joint is typically about 25 μm thick. Fig. 18(C) shows that the BR 127 epoxy wets the PZT surface well. The bright clumps in the epoxy are silver powder.

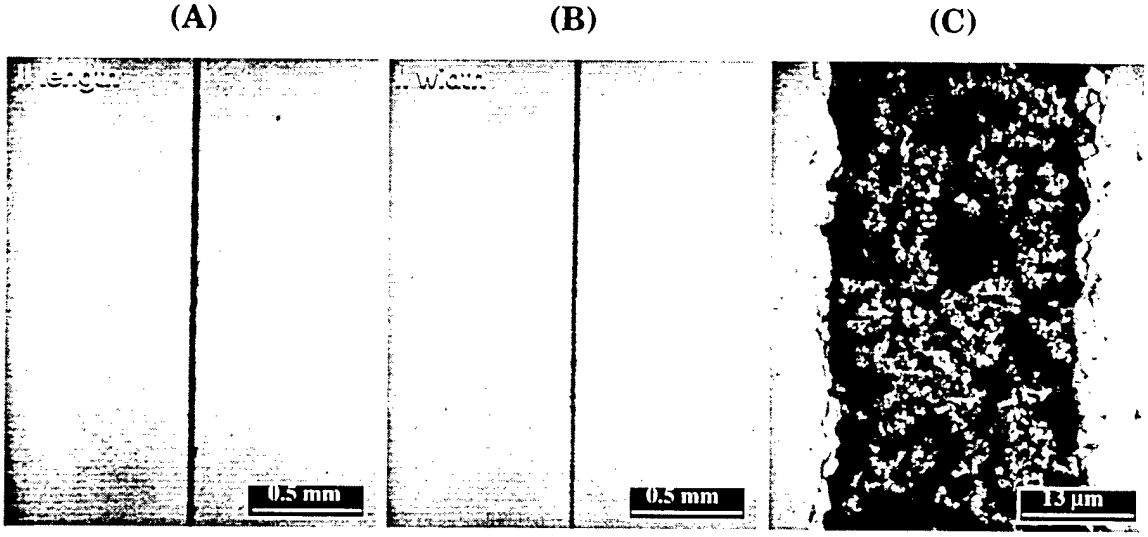

Fig.18 SEM micrographs of PZT joints bonded using 'standard' procedure- Ag loaded BR127 epoxy on one side and BR127 on the opposite side.

2.3.2 NDT Evaluation of Assembled Tubular Element by Electric Impedance Analysis

A torsional actuator was assembled at NRL with L=2.5" and R=0.5" using EDO PZT-5A segments as shown in Fig. 19. The electric impedance of the actuator is shown in Fig. 20 where a series of resonant frequencies were observed. From the sample dimension, it can be concluded that the lowest resonance is the fundamental shear resonance along the length direction (along the axial direction of the actuator). In the impedance

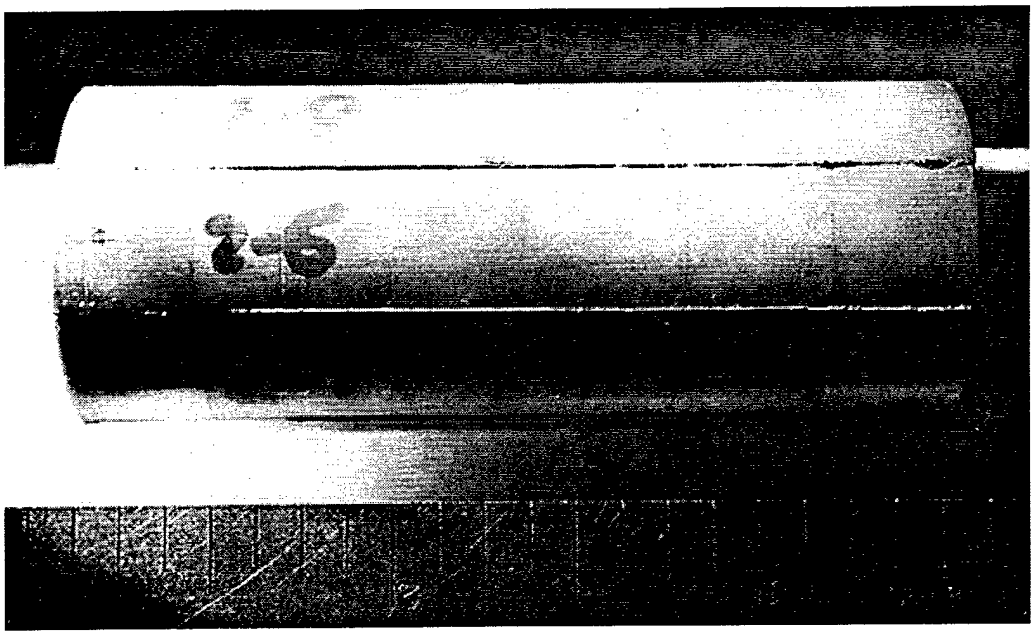

Fig.19 Assembled torsional actuator tube using PZT 5A segments.

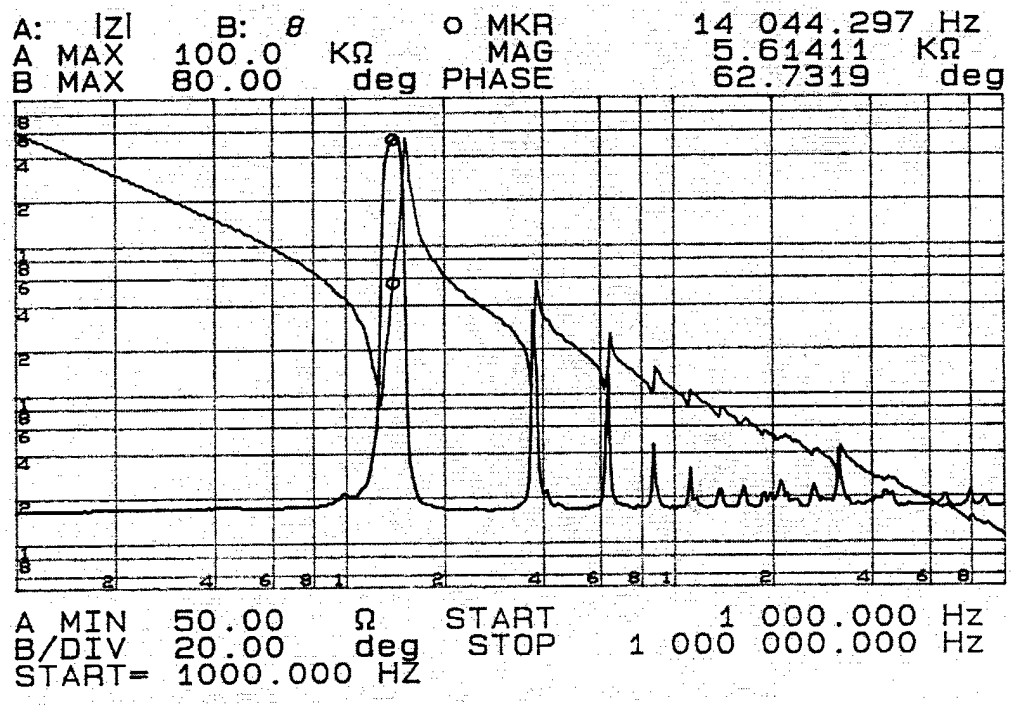

Fig.20 The electric impedance of the actuator tube #1 showing a series of resonance.

resonance frequency to the observed 14.5 kHz from the theoretical value of about 17 kHz when both ends of the actuator are free. There exist many higher harmonics as shown in Fig 20. The sharp resonance peak at 14.5 kHz indicates that the whole tubular actuator acts as a single unit, implying a relatively high quality of joints between the segments. For a single segment which has 1 cm width (the same as those in the actuator), the fundamental resonance will be at about 114 kHz (the shear velocity for PZT-5A is about 2270 m/s). If the joint between some segments is not very good, one would expect to observe resonance at a frequency near that. This fact provides a very convenient means to test the quality of the joints. In addition, the resonance method can also be used to test the actuator after the load test. If there is a fracture in the actuator, the resonance spectrum will be very different from that before the fracture.

2.4 Element Performance Characterization

2.4.1 Shear Coefficient Evaluation of Individually Poled Segments

Prior to the evaluation of the prototype torsion actuator element, two continuously poled PZT-5A segments were tested to determine the d_{15} shear coefficient. As shown in Fig. 12, there is no large difference in d_{15} at a low field level. However, as the driving field strength increases, the difference between sample #9-8 (d_{33}= 444 pC/N) and #9-6 (d_{33}= 420 pC/N) becomes significant. In addition, the piezoelectric response of the EDO PZT-5A poled at NRL using the continuous poling method is compared with that poled by the manufacturer and the results were presented in figure 5(c). The behavior of sample 9-8 (black dots) is the same as that poled by the manufacturer (open triangles) with a d_{33}= 450 pC/N. However, the sample 9-6 is a little lower than both EDO 9-8 and the one from the manufacturer. This lower d_{15} must be due to the smaller electrode spacing used in the continuous poling process of sample 9-6 case

(refer to Section 2.1.4). The poling electric fields for samples 9-8 and 9-6 were 25 kV/1.2 cm and 15 kV/0.7 cm, respectively.

As shown in Table I, in the stress free condition, PZT-5A (EDO), PZT-5H and N-21 are the three best materials choices. Among them, PZT-5A has the highest Curie temperature. Using the extrapolated shear coefficient d_{15}= 2,200 pC/N at 4 kV/cm for the EDO PZT-5A (Fig. 21), the blocking torque in Section 2.1 is 480 in-lb which meets the MD 900 helicopter rotor blade twist requirement. Using the same shear coefficient, the actuator can also meet the ± 4° twist angle requirement for the trailing edge flap of the helicopter with an assembled tube's length to diameter ratio of 20.

2.4.2 Assembled Tubular Element Performance Characterization

The torsional angle of the actuator was characterized as a function of the external field strength and frequency. The measurement was carried out without load using a laser light reflection method as shown in Fig. 22. With actuator tube #1, the torsional angle β was plotted as a function of applied electric field as shown in Fig. 23. Under a field of 2 kV/cm β is about 0.06°. Since the depoling field for the material is above 4 kV/cm and there is a strong non-linearity in the piezoelectric shear response at a field of approximately 4 kV/cm, an extrapolated value of 0.32° for the angle β at 4 kV/cm is conservative. Hence, using the current material, with 7 actuators in series, an angle of more than 2° can be achieved. In the current actuator configuration, the angular amplification factor is 5 (L=2.5" and R = 0.5"). From the equation: $\beta = d_{15} E L/R$

where β is the torsional angle measured, d_{15} of the material can be deduced and plotted as shown in Fig. 24. The data in Fig. 24 is quite similar to that in Fig. 2B except at low fields (300 V/cm). This could be due to errors in the current apparatus in measuring small torsional angles. Nevertheless,

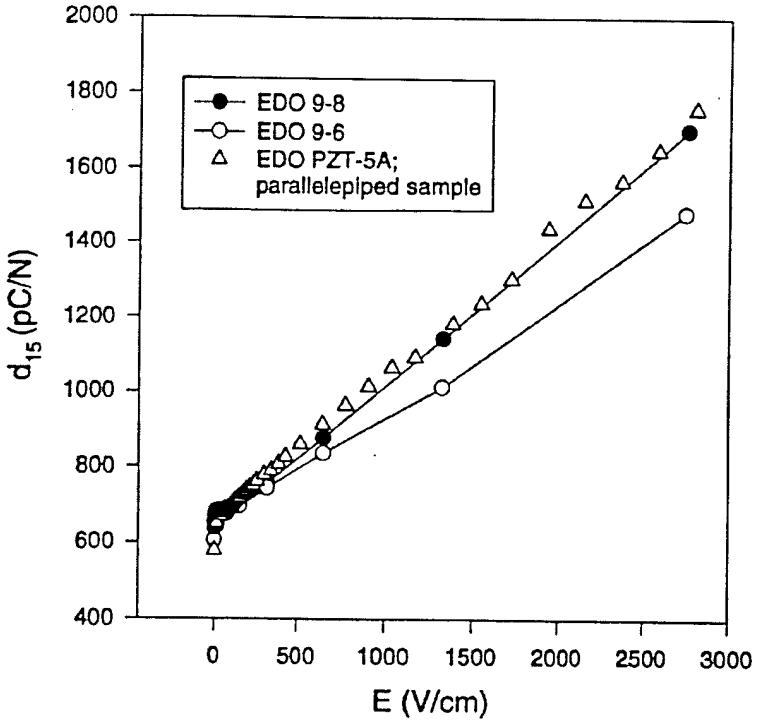

Fig. 21 d_{15} shear coefficient of the continuously poled PZT-5A segments as a function of applied field strength.

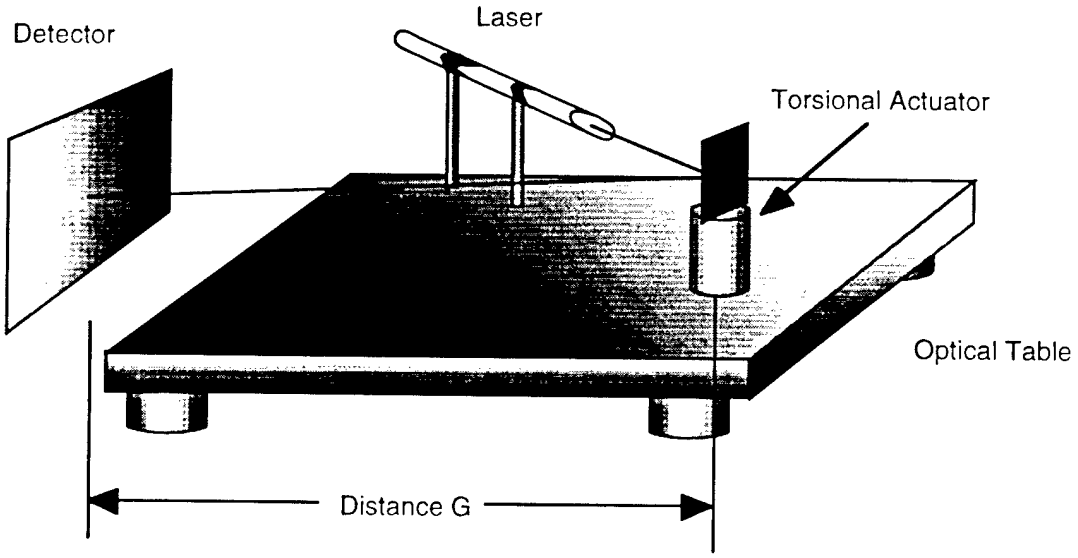

Fig. 22 Schematic of laser light reflection set up

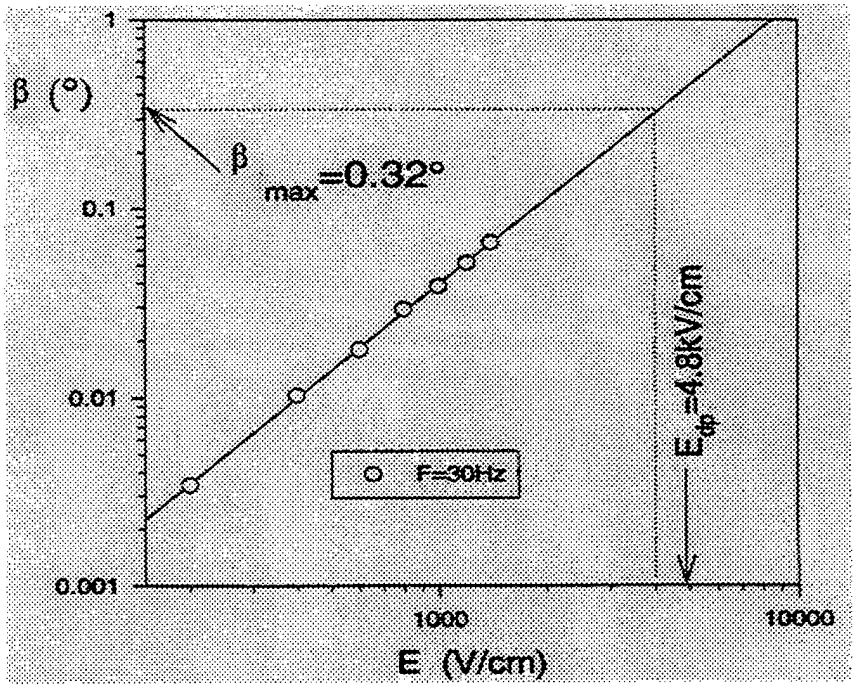

Fig. 23 Torsional angle β of actuator tube #1 as a function of applied field.

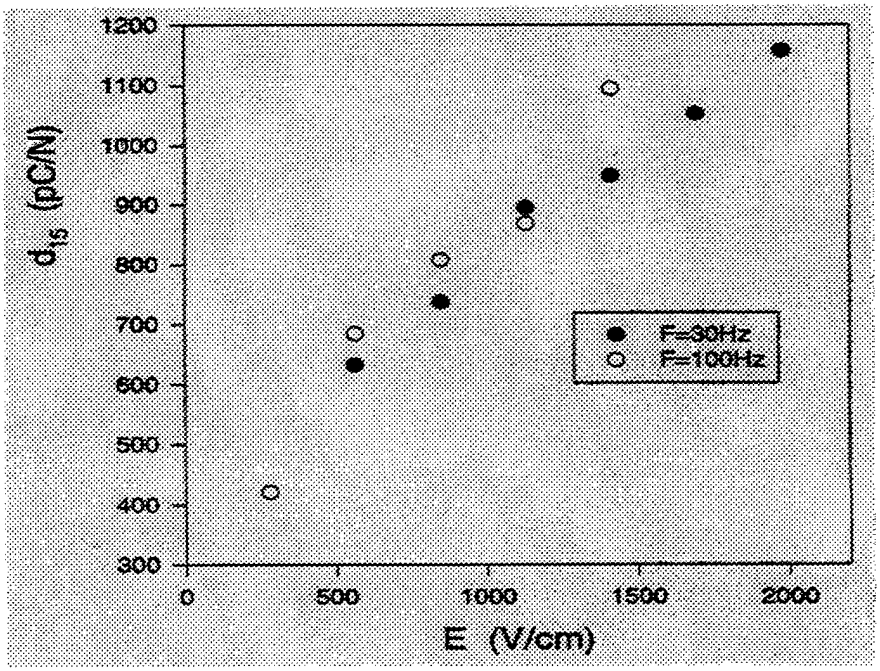

Fig. 24 d_{15} of actuator tube #1 plotted as a function of applied field

this result is a clear verification of the concept of using d_{15} and angular amplification to generate large torsional motion. The next step in the investigation is to test the torsional actuator under load.

2.5 Modeling for Performance Prediction

2.5.1 Basic Shear Response and Electric Field Effects

Analytical models were developed to examine the effects of a changing electric field orientation on the shear deformation of a piezoelectric element. Two electric field conditions were examined: electric fields of uniform magnitude in a plane perpendicular to the polarity vector for the material and non-uniform electric fields. It was concluded that, if the field has a constant magnitude, the shear acts in the plane containing the electric field and the polarization vector. The resulting shear deformation is well behaved. An applied non-uniform field results in a more complex deformation pattern. The deformation results in a concave profile of the piezoelectric segment. Finite element models were then developed to examine the effects of changing electric field orientation on the shear deformation of a beam of rectangular cross section. Two support conditions were considered: a cantilever beam and a beam supported at one point. The same electric field orientations examined in the analytical models were applied to the finite element beam models. Computationally determined stress, strain, and deformation fields were verified with the analytical models described in the report, "Basic Shear Response and Electric Field Effects" by Diann Brei, University of Michigan.

2.5.2 Modeling of Thin-Bond Segmented Cylindrical and Polygonal Actuators

The next stage of the modeling effort centered on capturing bond effects for more realistic, 3-D actuator geometries and loading these geometries with a back torque. A computer code was written which automatically

generates a finite element model for a given torsional actuator from a prescription of the actuator's parameters. Use of this code in conjunction with ABAQUS has lead to some preliminary results. The first study involved a comparison of 40 and 60 micron bond thicknesses in torsional actuators of polygonal cross sections. The second involved a performance curve comparison of a cylindrical torsional actuator with one whose cross-sections were equal-sided polygons while the other parameters were being held constant. Further studies involving a wider range of parameters, as well as stress and/or strain distribution comparisons, are planned.

The range of geometric shapes contemplated for torsional actuators is rather limited (cylinders or equal-sided polygonal cross sections), but other model parameters, such as actuator length, are each associated with a range of possible values. Rather than building a multitude of such models "by hand", this scenario suggests a specialized, parameter-driven automation of the model building process. BONSAI, which stands for BONded-Segment Actuator Interpreter, is an ABAQUS language extension which was written just for such a purpose. (It's name is a metaphor if one thinks of large, general-purpose ABAQUS preprocessors, such as PATRAN, as "full size".) It is written in Mathematica and takes the form of a preprocessor. As implemented, it translates parametrized macros (special Mathematica expressions) embedded within an ABAQUS-input template into an ABAQUS input (.inp file). The macros of BONSAI are designed to allow the user to build and manipulate ABAQUS models of torsional actuators by merely providing the desired parameter values associated with the specific model. The mesh transitioning is governed by an input parameter which sets the "aspect ratio" between (transitioned) mesh size transverse to the bond versus mesh size tangential to the bond. Multiple-point constraints (MPC's) are automatically generated by BONSAI to facilitate the transitioning. The bonds are strictly of uniform thickness and there are no vertices at the bond exterior faces which might otherwise act as artificial stress concentrators for the polygonal case. BONSAI generates true three dimensional models consisting of C3D20E

(20-noded brick) piezoelectric elements. Artificial "caps", attached to each end of the actuator model, act as rigid insulators through which mechanical loads and/or constraints can be interfaced to the actuator. The actuator can be mechanically loaded or constrained by mechanically loading or constraining degrees-of-freedom 1 through 3 (for displacement) and/or 4 through 6 (for rotation) of the outer-surface center for each end-plate. (The centers are denoted by node sets xmincntr and xmaxcntr.) Electrical loading of the actuator is accomplished by specifying an electrical potential value for degree-of-freedom 9 of the node set epotbond (of the ABAQUS input generated by BONSAI). Periodicity (with rotation) in the solution for the N-sided case allows for the FEM modeling of only an Nth of the actuator's total circumference. A serendipitous benefit of this overall effort has been an original contribution to the generic problem of node transitioning, with a technical note planned for journal submission. An example ABAQUS template, with embedded BONSAI macros, is given in Table IV.

As a benchmark and check on the output of BONSAI, two of the models (FRL1W1H10L and TRL1W1H10L) contained in Diann Brei's report were generated using BONSAI with a variety of meshes. The ABAQUS results of the BONSAI-generated models were consistent with the results of Diann Brei's report.

The first study consists of cases of 40 microns and 60 microns for bond thickness. For each bond thickness, the model was first loaded with 1600 V to the bond (assumed to be a conductor) and then 5000V. No mechanical back torque was applied. (Adjacent bonds in the actuator model have -1600 V or -5000 V applied to them, respectively, so that the bonds alternate between positive and negative applied voltage of the same magnitude as one moves around the actuator.) For these models, the value of 1600 V on the bond leads to electric field values of approximately 4 kV/cm, a nominal value taken from Section 2.1.1. The poling of the piezoelectric segments is also periodic, with the poling alternating between adjacent segments. The ABAQUS POST output included in this report is

TABLE IV: ABAQUS INPUT TEMPLATE WITH BONSAI MACROS

```
**
*HEADING
piezo model, 1600V bond, fixed left, 0 torque right, 60 micron bond
**
*RESTART, WRITE, OVERLAY
**
<*      BondedSegmentActuator[ GeometryAndMesh[
                    IsCylindrical->False,
                    SegmentPeriod->8,
                    InnerRadius->(((13/32) 2.54) (10^(-2))),
                    BondThickness->(6 (10^(-5))),
                    Length->(2.54 (10^(-2))),
                    SegmentThickness->((2.54/8) (10^(-2))),
                    MeshAspectRatio->25] ]  *>
**
<*
BondedSegmentActuator[ Materials[
        YoungsModulusBond->(4.76 (10^(9))),
        PoissonsRatioBond->(0.288),
        YoungsModulusPiezo->(5.3 (10^(10))),
        PoissonsRatioPiezo->(0.25),
        DielectricCoeffPiezo->(1.5 (10^(-8))),
        PiezoStrainCouplingPolePolePoleComp->(374.0 (10^(-12))),
        PiezoStrainCouplingNormtopoleNormtopolePoleComp->(584.0 (10^(-12))),
        PiezoStrainCouplingPoleNormtopoleNormtopoleComp->(-171.0 (10^(-12)))] ]  *>
**
*STEP,PERTURBATION
**
*STATIC
**
*BOUNDARY,OP=NEW
epotbond,9,9,1600.0
**
*BOUNDARY,OP=NEW
xmincntr,1,1,0.0
xmincntr,2,2,0.0
xmincntr,3,3,0.0
xmincntr,4,4,0.0
xmincntr,5,5,0.0
xmincntr,6,6,0.0
xmaxcntr,1,1,0.0
xmaxcntr,2,2,0.0
xmaxcntr,3,3,0.0
xmaxcntr,5,5,0.0
xmaxcntr,6,6,0.0
**
```

for a model of an actuator whose cross section is an eight-sided polygon of equal sides. It has an inner radius of 13/32 inches and its walls are 1/8 inch (0.3175 mm) thick. The model is one inch long with the left end (x=0) of its length being fixed.

The piezoelectric material parameters were taken from Diann Brei's report for PZT-5A. The bond consists of a silver-inclusion, epoxy-matrix composite for which the following component properties are used:

Silver (1): Y=Young's modulus=70 GPa,

ν=Poisson's ratio=0.23,

V=volume fraction=0.17

Epoxy (2): Y=Young's modulus=4 GPa,

ν=Poisson's ratio=0.3,

V=volume fraction=0.83.

Simple rules of mixture were used to obtain composite bond properties: $Y=1/((V_1/Y_1)+(V_2/Y_2))$ and $\nu=(V_1\,\nu_1)+(V_2\,\nu_2)$. The bond extreme stress values, included in this report as Table V, were obtained from the corresponding ABAQUS .dat files. At 1600 V, the angular displacement at the free end is 0.0227676 degrees for the 40 micron bond thickness case, and 0.0227552 degrees for the 60 micron case. (The length to inner radius ratio is about 2.5 for these cases; previous reports envisioned ratios of about 100 for practical actuators.) Under no external mechanical loads, the 60 micron bond apparently does not degrade the performance of the actuator over that of the 40 micron bond.

The second study, whose results are summarized by Fig. 25, compares the performance of a polygonal geometry (regular octagon) versus a cylindrical geometry. The study is preliminary in the sense that stress and/or strain distribution comparisons, particularly at the bonds, as well as a wider range of actuator parameters, also need to be included. For the material/geometry parameters chosen, the blocking-torque versus angular-displacement curve of an equal-sided polygonal is close to that of comparable cylindrical actuator, with slightly better performance at the

TABLE V: EXTREMA OF BOND STRESSES

for piezo model, 1600V bond, fixed left, 40 micron bond:

ELEMENT	PT	FOOT-NOTE	S11	S22	S33	S12	S13	S23
MAXIMUM			1.4630E+05	4.5642E+04	5.2452E+04	1.5415E+06	3.8065E+04	7.7801E+05
ELEMENT			1	241	1	243	243	32
MINIMUM			-1.4630E+05	-4.5642E+04	-5.2452E+04	-1.2105E+06	-3.8065E+04	-4.7171E+04
ELEMENT			241	1	241	162	3	405

for piezo model, 1600V bond, fixed left, 60 micron bond:

ELEMENT	PT	FOOT-NOTE	S11	S22	S33	S12	S13	S23
MAXIMUM			2.0731E+05	7.1069E+04	7.3934E+04	1.3152E+06	5.0403E+04	7.5693E+05
ELEMENT			1	32	1	2	290	392
MINIMUM			-2.0731E+05	-7.1069E+04	-7.3934E+04	-1.1282E+06	-5.0403E+04	-4.1206E+04
ELEMENT			289	320	289	218	2	509

for piezo model, 5000V bond, fixed left, 40 micron bond:

ELEMENT	PT	FOOT-NOTE	S11	S22	S33	S12	S13	S23
MAXIMUM			4.5719E+05	1.4263E+05	1.6391E+05	4.8172E+06	1.1895E+05	2.4313E+06
ELEMENT			1	241	1	243	243	32
MINIMUM			-4.5719E+05	-1.4263E+05	-1.6391E+05	-3.7829E+06	-1.1895E+05	-1.4741E+05
ELEMENT			241	1	241	162	3	405

for piezo model, 5000V bond, fixed left, 60 micron bond:

ELEMENT	PT	FOOT-NOTE	S11	S22	S33	S12	S13	S23
MAXIMUM			6.4785E+05	2.2209E+05	2.3104E+05	4.1101E+06	1.5751E+05	2.3654E+06
ELEMENT			1	32	1	2	290	392
MINIMUM			-6.4785E+05	-2.2209E+05	-2.3104E+05	-3.5257E+06	-1.5751E+05	-1.2877E+05
ELEMENT			289	320	289	218	2	509

zero-displacement end of the curve and slightly degraded performance at the torque-free end of the curve. Example ABAQUS results for some of the models are included in this report in the form of undisplaced-displaced plots (Fig. 26A and Fig. 26B) and electrical potential contour plots (Fig. 27A and Fig. 27B). The plots were generated using ABAQUS Post. Further studies involving a wider range of parameters, as well as stress and /or strain distribution comparisons, are anticipated.

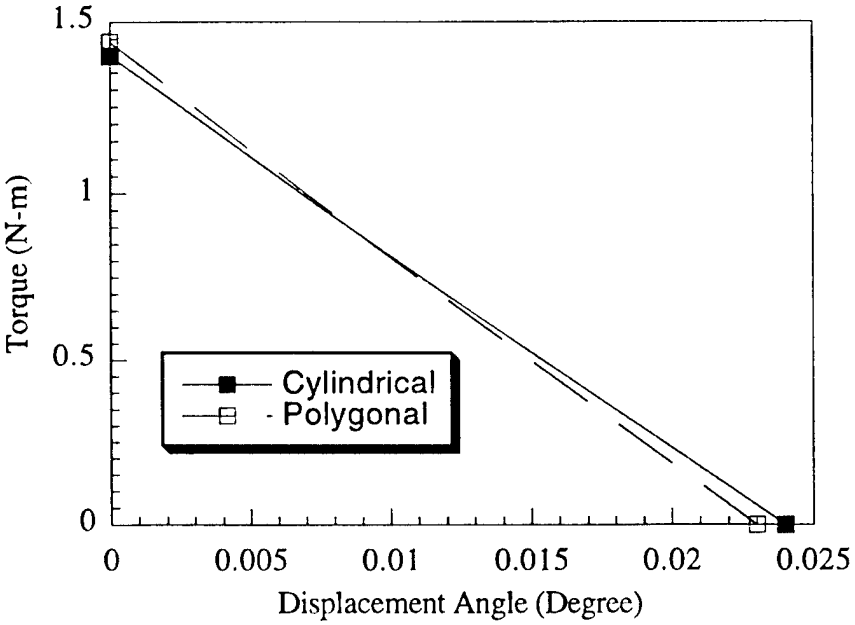

Fig. 25 Comparison of performance curves for 8-segmented torsional actuators of length 1 inch, inner radius 13/32 inch, wall thickness 1/8 inch, and bond thickness 60 microns.

2.5.3 Computational Simulation of Poling of a Piezoelectric Ceramic

Computational methods were used to examine the effects of the poling process on a candidate piezoelectric ceramic. Finite element techniques were used to generate a 2D model of a thin strip of PZT-5A representative of the sections to be used to fabricate the final torsional actuator (Fig. 28). The commercial finite element code ABAQUS was used for all analyses.

Three parametric studies were completed.

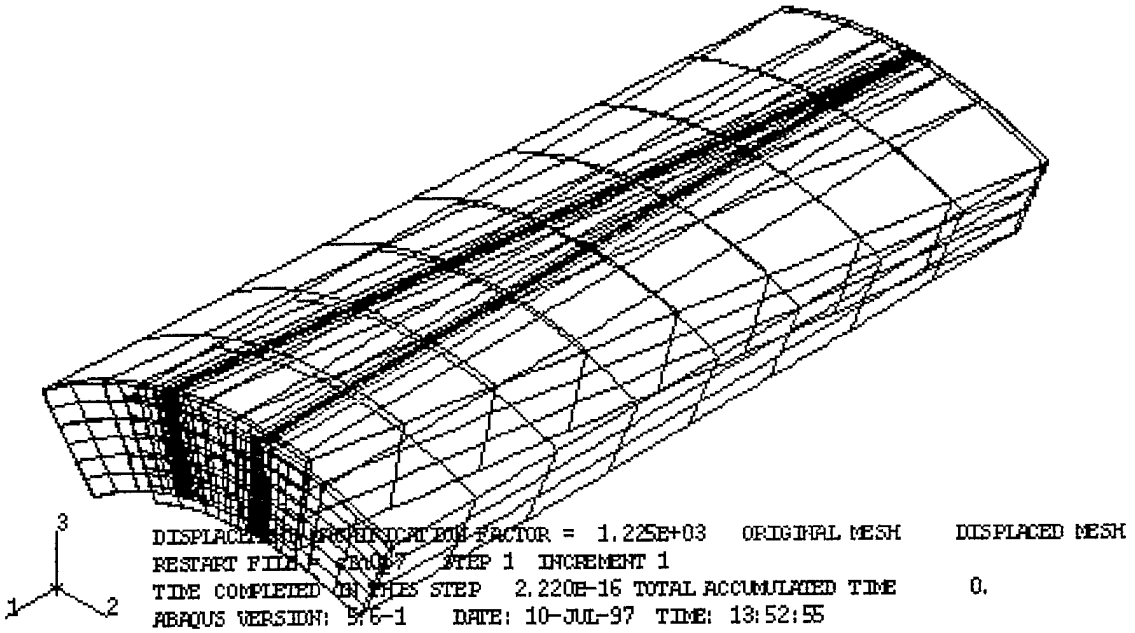

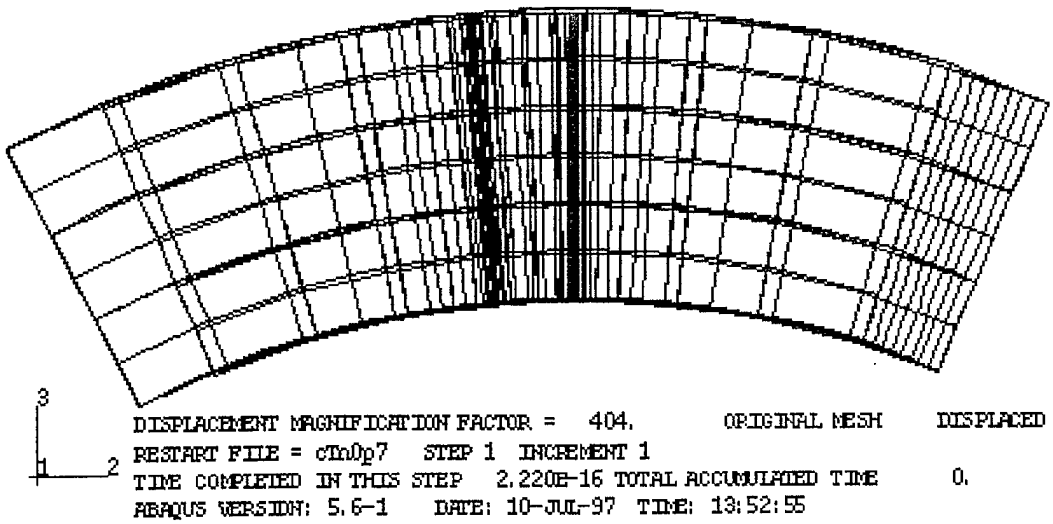

FIG. 26A: Plots of displaced/undisplaced meshes for case of 1600 V at bond, 0.7 N-m applied blocking torque, 8-segment cylindrical actuator: 0.01206 degrees angular displacement

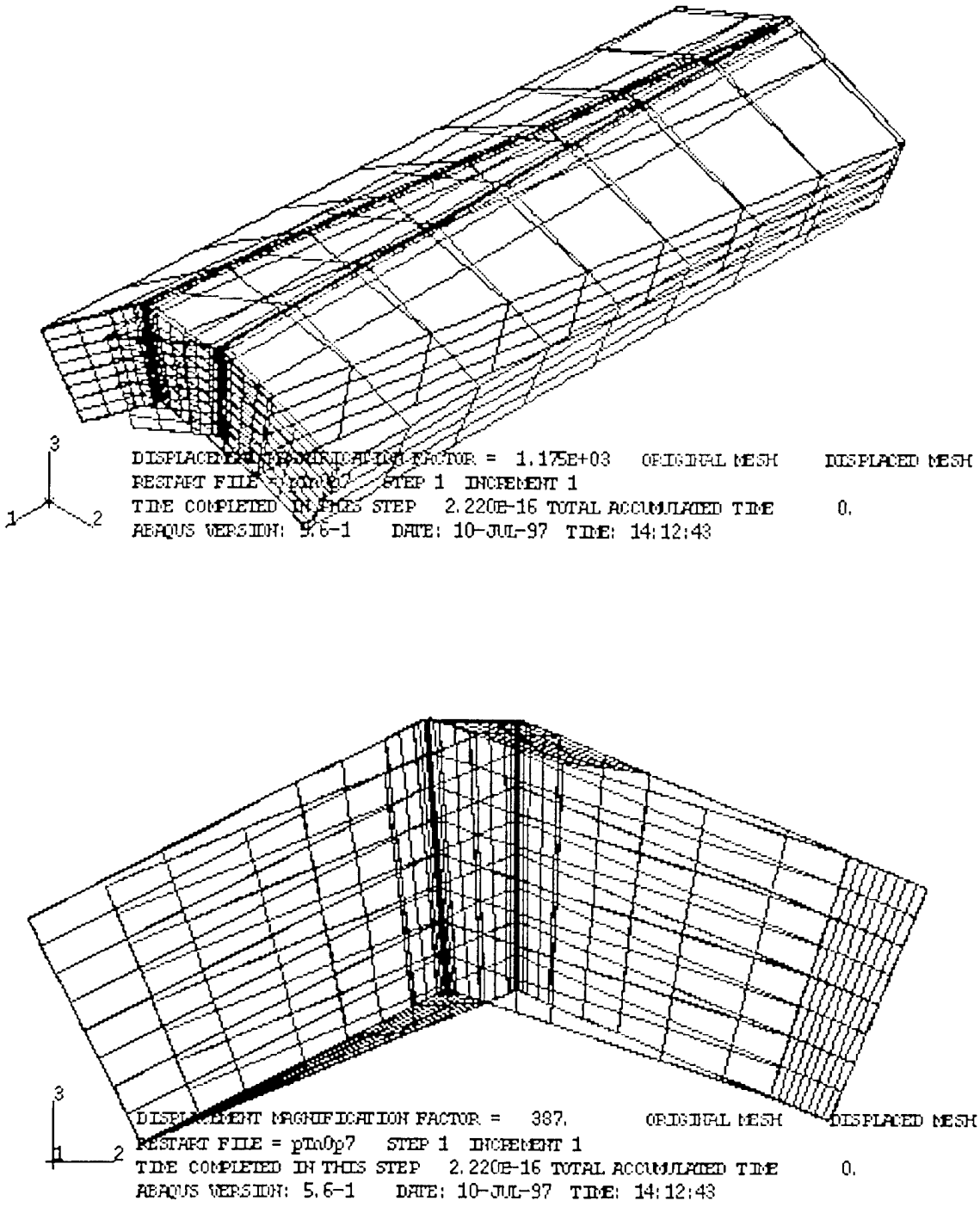

FIG. 26B: Plots of displaced/undisplaced meshes for case of 1600 V at bond, 0.7 N-m applied blocking torque, 8-segment polygonal cross section actuator: 0.01164 degrees angular displacement

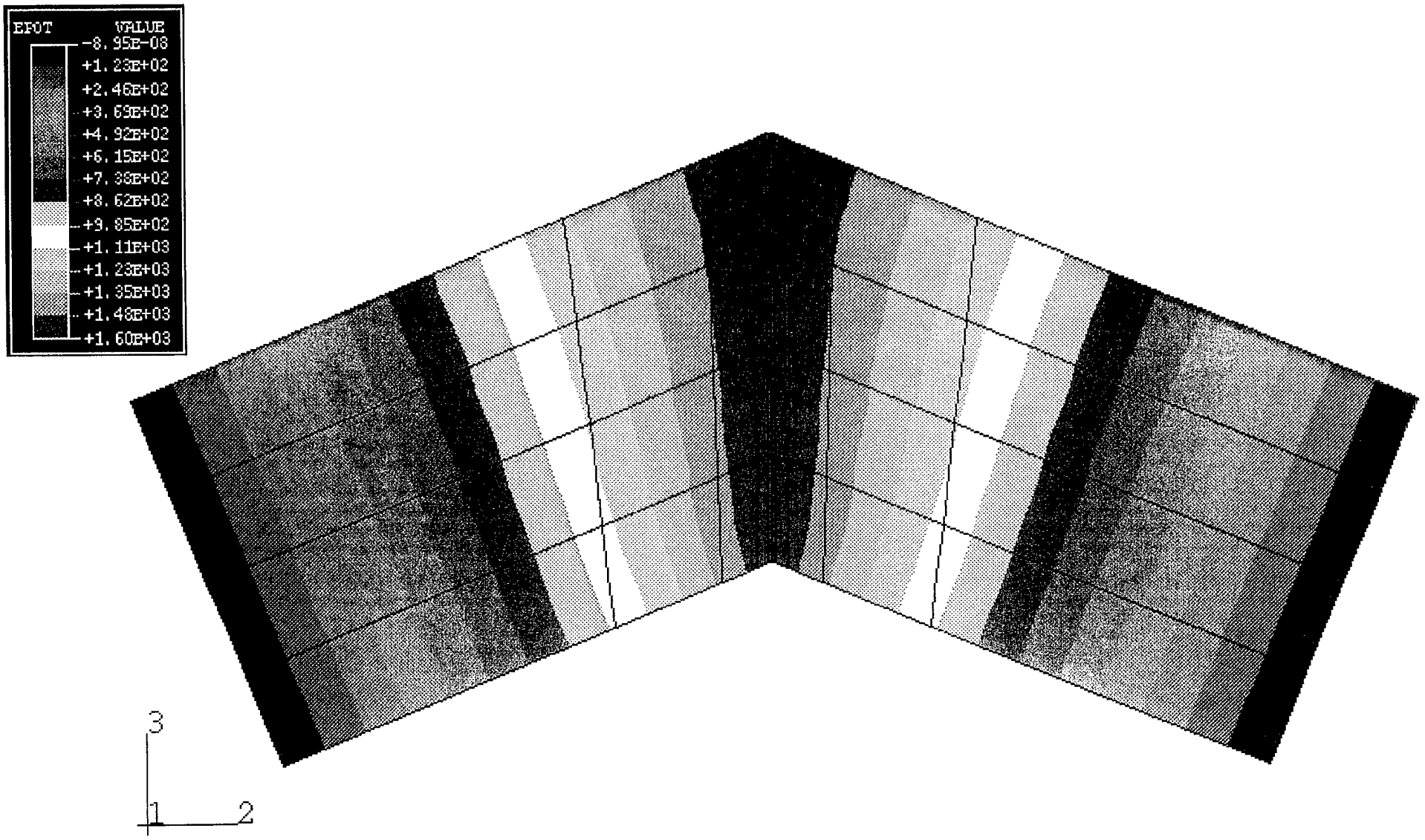

FIG. 27B: Contour plot of electrical potential at cross section 0.01 m from fixed end for case of 1600 V at bond, 0.7 N-m applioed blocking torque, 8-segment polygonal cross section actuator

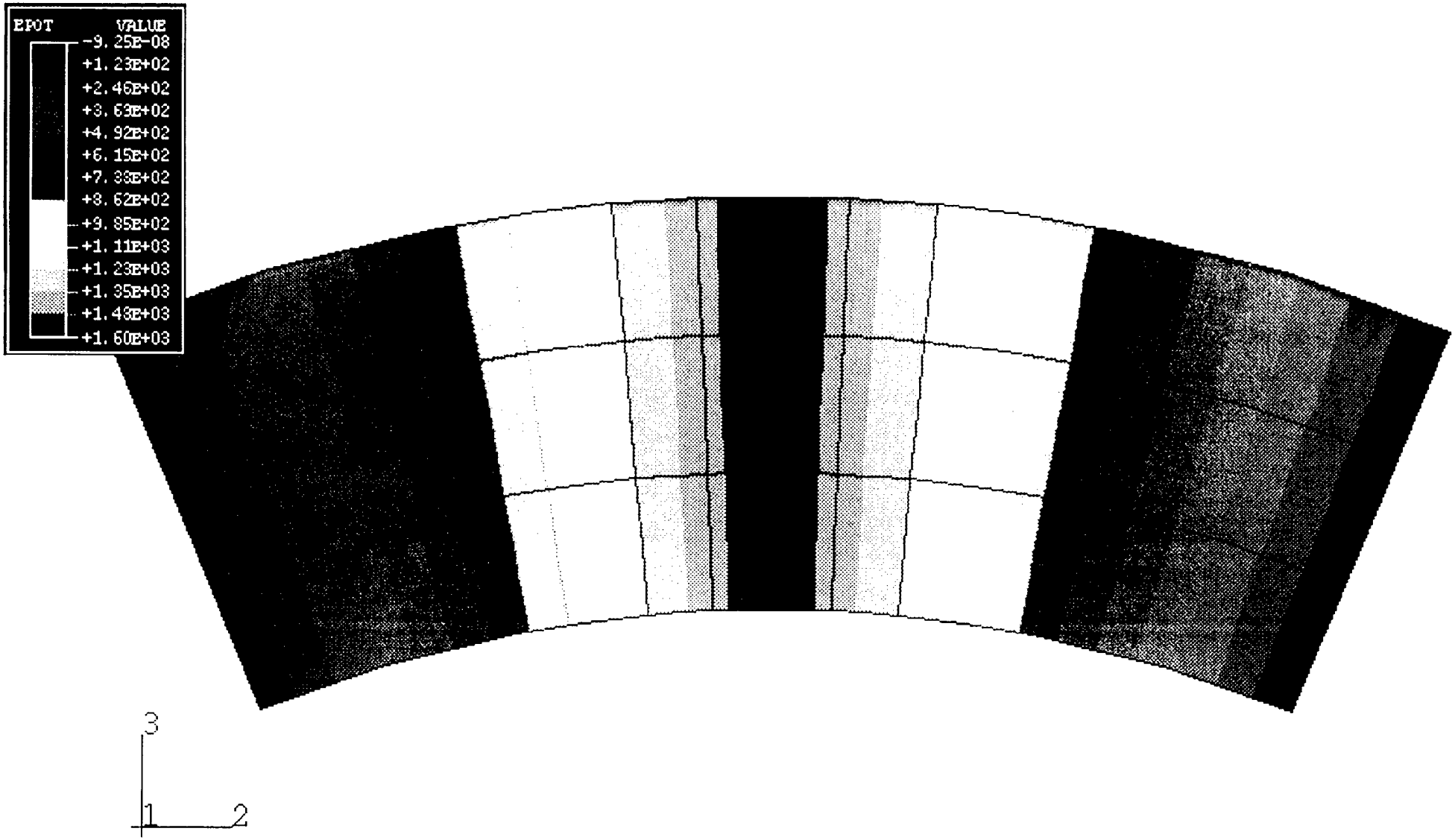

FIG. 27A: Contour plot of electrical potential at cross section 0.01 m from fixed end for case of 1600 V at bond, 0.7 N-m applioed blocking torque, 8-segment cylindrical actuator

The first study examined electrode spacing and the electric field developed in a specimen of virgin non-poled material as a result of an applied field. Electrode spacings of 5, 10 and 20 mm were examined.

The second study examined combining poled and non-poled materials. Material in the specimen modeled is defined as either poled or non-poled. No provision is made for the modeling of partially poled material. Five combinations were examined for an electrode spacing of 20 mm. Material combinations considered are: (1) all non-poled material, (2) half poled and half non-poled with the division at the centerline between electrodes, (3) 1/4 poled and 3/4 non-poled (4) 3/4 poled and 1/4 non-poled and (5) all poled material. These combinations are a simplification of the complex combinations of non-poled, partially poled and poled material which occur during the process. Electric fields and internal stresses are calculated for application of 1.0 kV/mm and 2.0 kV/mm electric fields and electrode spacings of 5, 10 and 20 mm.

The third study examined differences in calculated electric fields and internal stresses resulting from two poling procedures. The effectiveness, or amount of material poled, is evaluated for both procedures. The first procedure consists of one application of a high electric field. The second procedure consists of two sequential applications of a lower electric field. The electrode spacing is 10 mm. Applied fields are 2.0 kV/mm for one pass poling or 1.0 kV/mm for two pass poling. Electric fields for the processes are shown in Fig. 29. The material poled for each of the two processes is shown in Fig. 30.

General conclusions obtained from reviewing the computational results are:

(1) The spacing of electrodes affects the interaction of electrical fields. Closer electrode spacing increases the magnitude of the field experienced by the specimen.

(2) Field and stress discontinuities occur at the interface between poled and non-poled material.

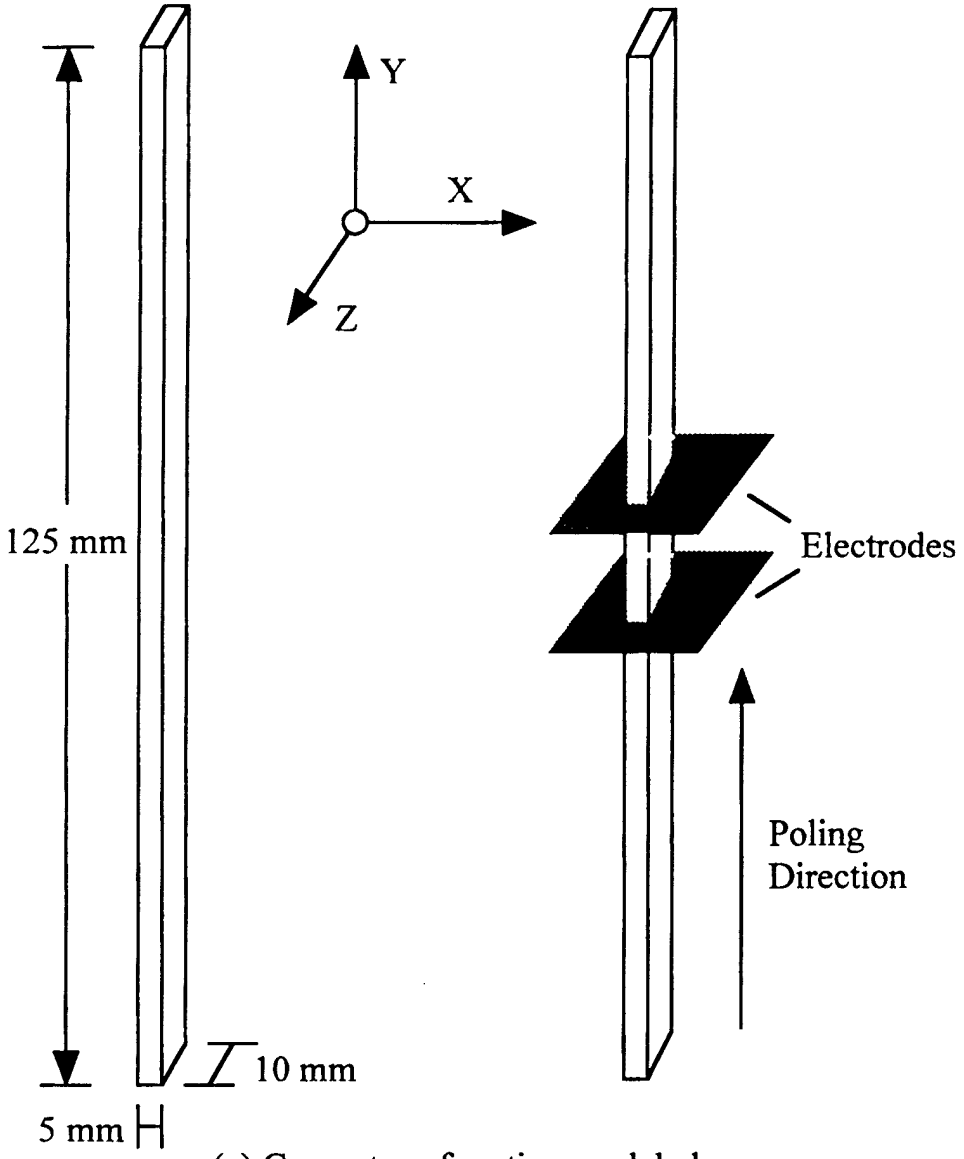

(a) Geometry of section modeled

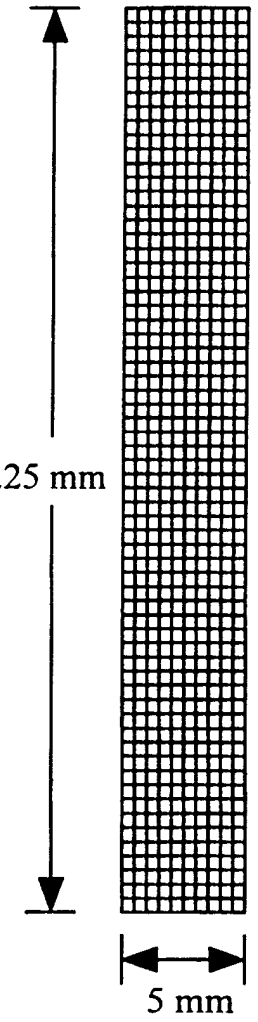

(b) Close up of mesh in region of electrodes

Fig. 28 Geometry and finite element mesh for continuous poling study

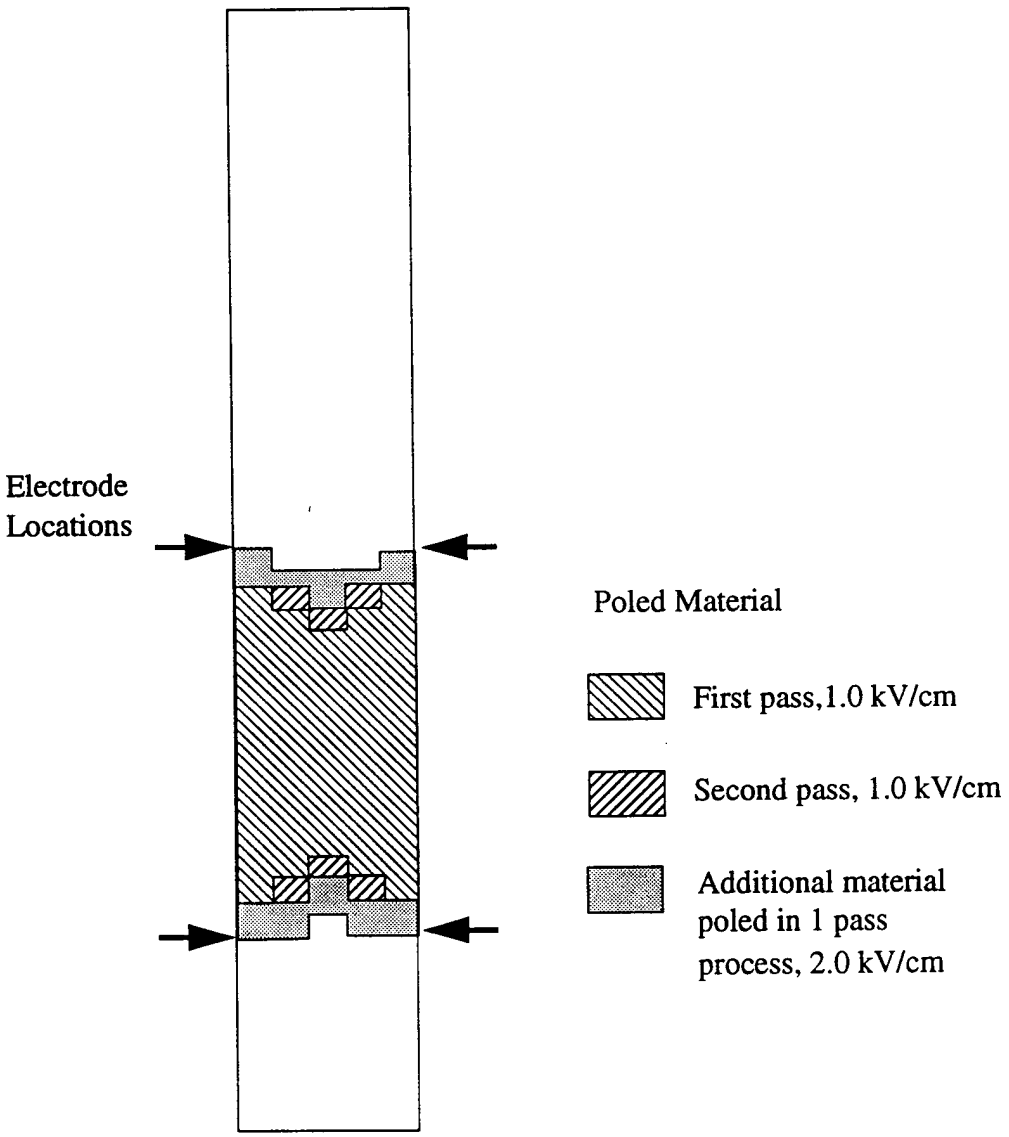

Fig. 29: Material poled as a result of the application of field, one and two pass poling processes. Material considered poled when calculated field > 0.80 kV/mm.

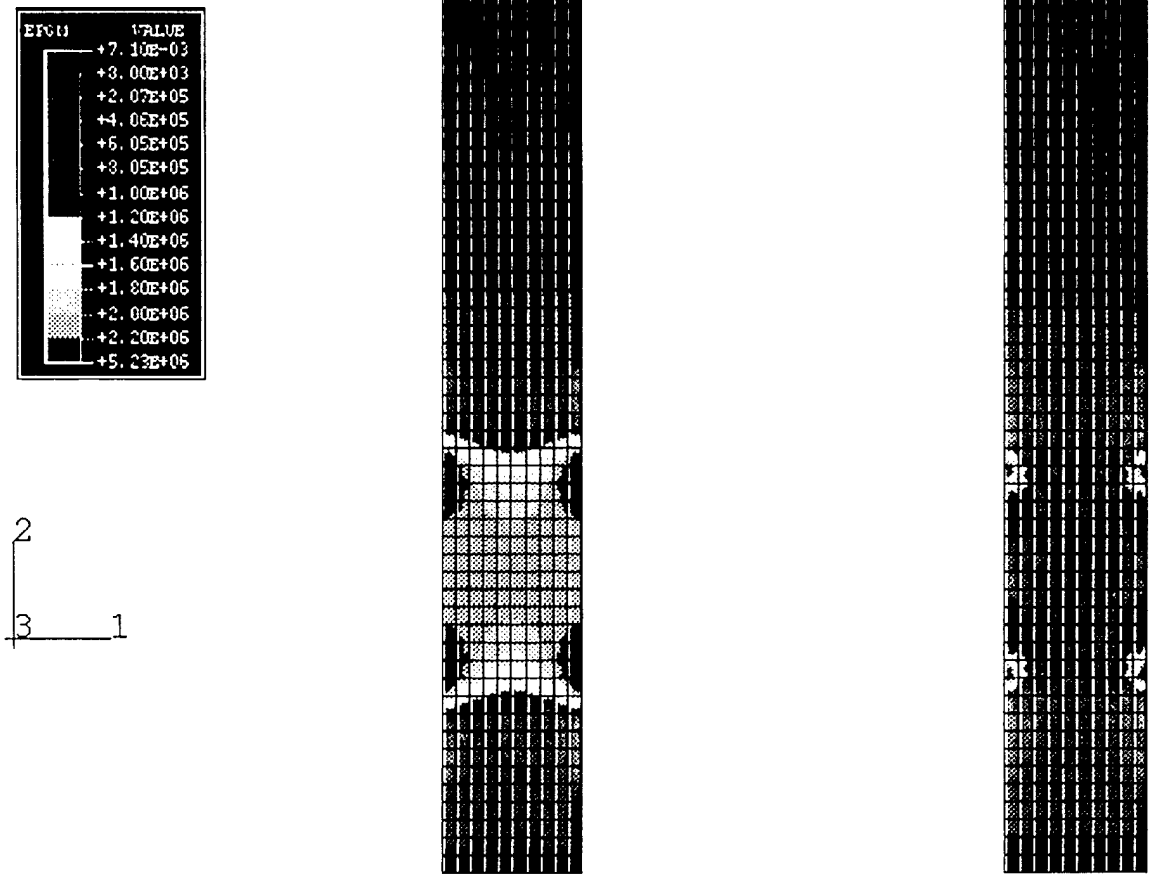

(a) One pass process
2.0 kV/mm
All non-poled material

(b) Two pass process
1.0 kV/mm
Pass 2, poled and non-poled material

Fig. 30 - Electrical field during poling process

(3) Poled material has significantly higher stress levels resulting from a reapplication of a poling field.

(4) In the comparison of a two pass and one pass poling process, it was found that the one pass process results in lower stresses and a larger area of material obtaining the electrical field required for poling.

The presence of poled material in the section being poled is important. Stress levels increase by more than an order of magnitude due to the presence of poled material. The poled material responds to the applied electrical field according to its piezoelectric properties. Non-poled material is unresponsive to the applied electric field. When the surrounding material does not respond to the electric field, the active material is restrained and high stresses result.

2.6 Prototype Actuator Design, Fabrication and Testing

The prototype torsional actuator configuration can be the same as what was used in the single tube actuator element. However, in order to build a long actuator as required for certain applications such as a helicopter rotor blade, the PZT segments should be long and/or be able to be extended by adding several segments. The latter approach is desirable because there exist practical limits to make long segments or long tubes. The preparation of long segments from long tubes is difficult and costly. Consequently, an alternate practical approach involves employing trapezoidal segments. With these, one can build a polygonal configuration actuator as shown in Fig. 31. The excess material in polygonal configurations over the cylindrical one decreases as the number of the sides of the regular polygon increases. The more sides the regular polygon has, the less excess area (material). (The finite element analysis in Section 2.5.2 indicated that the performance curves are comparable of octagonal and cylindrical configurations. The regular octagonal configuration yields about 5% less angular displacement than the cylindrical one in the load free condition. It is predictable that the discrepancy in angular displacement and torque will also be smaller as the

number of sides of polygon increase. Depending on the degree of discrepancy, there may not be a need to remove the excess material from the polygonal geometry.)

The flow chart of the prototype torsional actuator fabrication process is shown in Fig. 32. As described in previous sections, the initial attempt to make an actuator proceeded in the following order: selection of PZT tubes, cutting into segments, poling, electroding, joining, and assembling into tubular actuator elements. Two tubes have been assembled. The first was assembled using TRA-DUCT 2902 conductive silver epoxy. The second was assembled using Ag powder loaded BR127 primer epoxy and consolidated using the vacuum bagging process. The manufacturing process is undergoing constant revision for optimum results.

3 SUMMARY OF PROGRESS DURING THE LAST 12 MONTHS:

T1: Design, materials selection, segment preparation, and continuous poling

- Tubular actuator elements of lead zirconate titanate (PZT) ceramics were designed in a segmented configuration chosen for optimum shear response.
- Materials selections are PZT-5A, PZT-5H and N21 as determined from the initial evaluation of PZT materials based on their shear response to applied electric fields conducted under stress free conditions. The materials evaluation included determination of the non-linear response and the depoling limit.
- Evaluation of PZT materials was conducted based on their shear response to applied electric fields under stress up to 10 MPa.
- PZT-5A tubes were cut longitudinally into eight equal segments from each tube for the preparation of single tube actuator elements.
- Optimum poling conditions were established for the conventional oil bath poling on the selected PZT materials.

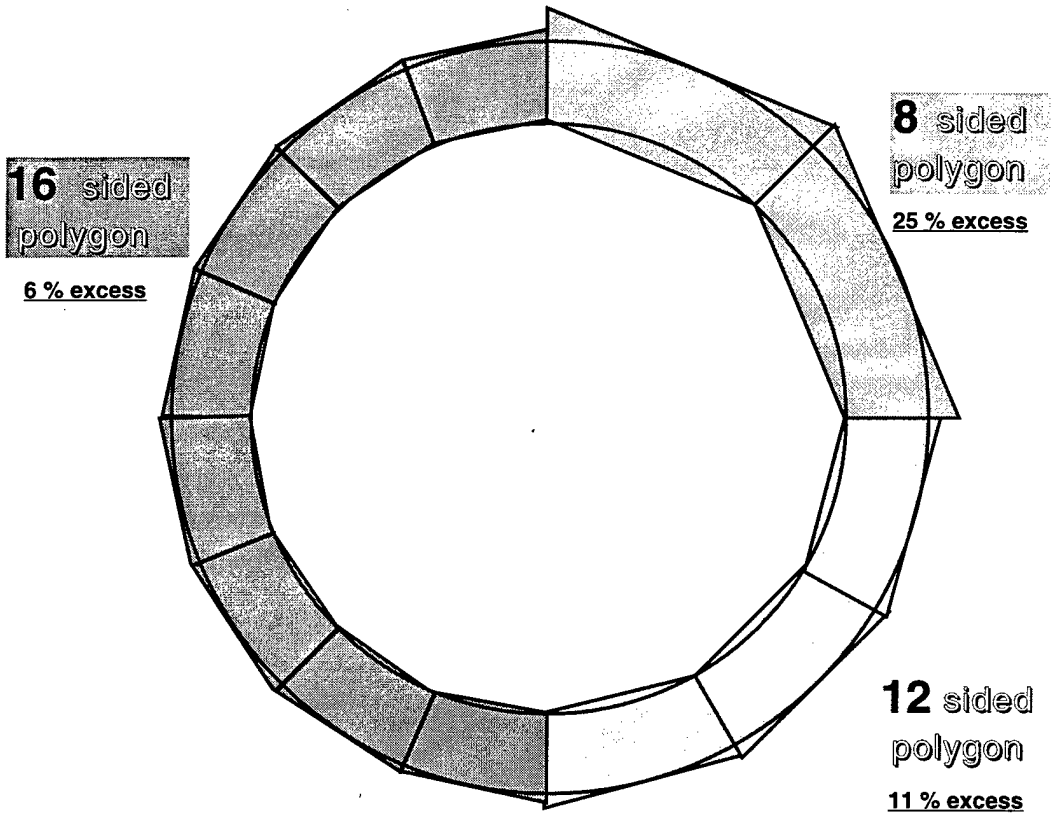

Fig. 31 Comparison of cylindrical and polygonal cross section areas.

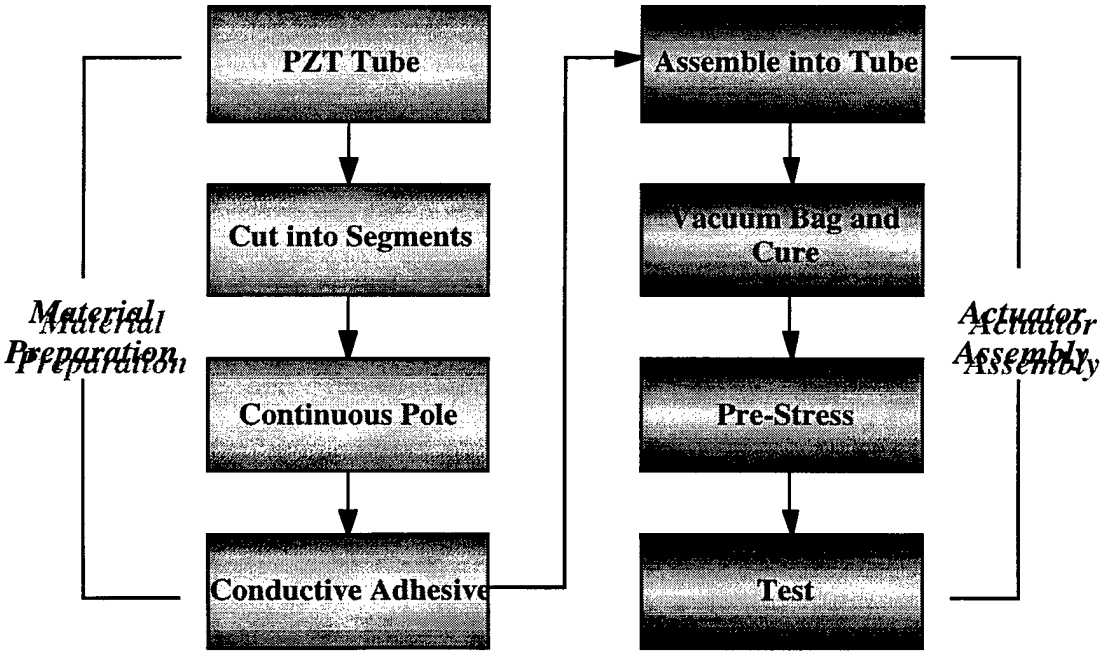

Fig. 32 Torsion actuator manufacture process flowchart

• A continuous poling technique was developed for effective poling of long PZT segments.

• An electric dipole model was used to predict the poling behavior of PZT materials. Predictions of the model were verified with experimental data.

T2: Electroding and joining of segments into a tubular actuator element

• A preliminary study on electroding and joining of materials was conducted. A series of bonding materials were evaluated by shear testing to determine the effect of surface conditions and electrode coatings.

• Shear strength test of the test coupons of the joints made with Tra-con Ag epoxy and BR127 primer epoxy failed throught the PZT ceramic body indicating the shear strength of the joints are higher than that of the PZT.

• A pulsed induction joining investigation was also conducted.

T3: Microscopic characterization and NDT analyses

• Microstructural characterization on electroding and joining of PZT segments was conducted. SEM fractographs and metallographs revealed the joining integrity of joint materials including Tra-con 2902 conductive Ag epoxy and Ag powder loaded BR 127 primer epoxy.

• Tensile fracture fractographs showed typical debonding (failure) in both adhesive joints as well as occasional air pockets in the joint.

• Electric impedance analysis on the assemled actuator tube was conducted. The resonance peaks indicated that the whole unit acted as a single unit, implying a relatively high quality of joints between segments.

T4: Element performance characterization

• Two continuously poled PZT-5A segments were tested to determine the d_{15} shear coefficient. The d_{15} response at 3 kV/cm field strength showed 1,800 pC/N which is a factor of three increase over that at low fields.

• Assembled actuator tubular element (tube #1) yielded torsional angle of 0.06 degrees under a field of 2 kV/cm. The torsional angle was estimated to be 0.32 degrees at 4 kV/cm.

T5: Modeling for performance prediction

• Analytical and finite element models were developed. Fields of constant magnitude but varied orientation in the plane perpendicular to the polarity vector of the material result in shear acting in the plane containing the electric field and the polarization vector. Non-uniform fields result in more complex deformation patterns.

• A computer code was developed to analyze joint thickness effects and actuator segment configuration effects on 3-D ABAQUS models. Preliminary results show that there is not a significant difference in performance between 40 and 60 μm joint thicknesses (under load-free) and performance curves between cylinder and polygon actuator configurations.

• A finite element study on continuous poling of piezoelectric material was conducted. The effects of electrode spacing were evaluated in terms of calculated fields and internal stresses. Internal stresses and area poled were used as measures of effectiveness of proposed poling processes. The one pass poling process evaluated was determined to be the most effective.

T6: Prototype actuator design, fabrication and testing

• An initial design concept has been established based on the polygonal configuration of the prototype torsional actuator. Fabrication techniques will be developed further when progress in Tasks 1-5 is more advanced.

4. PLANS FOR THE NEXT 12 MONTHS

- Properties of the potential candidate materials will be measured as functions of the applied mechanical load and electric field.
- The actuator design will be tailored to the requirements of particular applications, e.g. angular displacement, torque output, and physical size for helicopter rotor vibration control.
- Various electroding and joining techniques will be further explored, including adhesive bonding, brazing, and electron beam brazing/diffusion bonding.
- Single tubes small scale prototypes will be constructed using suitable materials selected on the basis of the measured property data and tested to validate the performance models (including twisting angles and load curves, and nonlinear field dependent behavior).
- Connection development to extend to 5 and 10 inches long tube.
- End coupling elements will also be developed.
- An evaluation will be performed on how the ceramic processing conditions, post-annealing, and grain size affect the shear strength of the ceramic material.
- New configurations of the torsional actuator, which can significantly simplify the assembling process and the cost of both the single tube and multi-tube actuators, will be developed
- Pre-stress the actuator using glass fiber reinforced wrap to improve the mechanical strength of entire tube.
- Computational modeling will be used to optimize actuator design for performance, fatigue resistance, and coupling to driven structures or systems.
- The effect of the number of alternating poled sections of curved and/or trapeizoidal configurations on actuator performance will be examined.
- Finite element techniques will be used to examine free end effects on poling process generated fields, stresses and strains. The effects of

electrode offset will be evaluated for poling. The presence of an electrical sink or cap at one end of the speciemn to be poled will be examined.

- Contacts for technology transfer will be initiated during this period.

5. ACKNOWLEDGMENTS:

This research program is being sponsored by Defense Advanced Research Projects Agency under DARPA Order No. D752. The authors (NRL) wish to thank Mark Chase, Robert Ingel, Kenneth Killian, Adam Gray, Timothy Yosenick, and Edward Chang for their assistance in the program. Also we thank Diann Brei (U of Michigan) for her initial modeling study, David Baird (EDO) for PZT-5A materials, and Ray Krieger and Jim Elliott (Cytec) for their suport in the BR127 joining experiment.

6. MILESTONE CHART